BBA - Bioenergetics 1864 (2023) 148984

Contents lists available at ScienceDirect

BBA - Bioenergetics

journal homepage: www.elsevier.com/locate/bbabio

Role of pheophytin *a* in the primary charge separation of photosystem I from *Acaryochloris marina*: Femtosecond optical studies of excitation energy and electron transfer reactions

Anastasia A. Petrova [a], Anna Paola Casazza [b], Ivan V. Shelaev [c], Fedor E. Gostev [c], Arseny V. Aybush [c], Victor A. Nadtochenko [c,d], Alexey Yu. Semenov [a,c], Stefano Santabarbara [b,e,*], Dmitry A. Cherepanov [a,c,**]

[a] A. N. Belozersky Institute of Physical-Chemical Biology, Lomonosov Moscow State University, Leninskye Gory 1 Building 40, 119992 Moscow, Russia
[b] Istituto di Biologia e Biotecnologia Agraria, Consiglio Nazionale delle Ricerche, Via Bassini 15a, 20133 Milano, Italy
[c] N.N. Semenov Federal Research Center for Chemical Physics, Russian Academy of Sciences, Kosygina Street 1, 119991 Moscow, Russia
[d] Department of Chemistry, Lomonosov Moscow State University, Leninskiye Gory 1-3, 119991 Moscow, Russia
[e] Photosynthesis Research Unit, Centro Studi sulla Biologia Cellulare e Molecolare delle Piante, Consiglio Nazionale delle Ricerche, Via Celoria 26, 20133 Milano, Italy

ARTICLE INFO

Keywords:
Photosystem I
Primary charge separation
Electron transfer
Femtosecond absorption spectroscopy

ABSTRACT

Photosystem I (PSI) of the cyanobacterium *Acaryochloris marina* is capable of performing an efficient photoelectrochemical conversion of far-red light due to its unique suite of cofactors. Chlorophyll *d* (Chl-*d*) has been long known as the major antenna pigment in the PSI from *A. marina*, while the exact cofactor composition of the reaction centre (RC) was established only recently by cryo-electron microscopy. The RC consists of four Chl-*d* molecules, and, surprisingly, two molecules of pheophytin *a* (Pheo-*a*), which provide a unique opportunity to resolve, spectrally and kinetically, the primary electron transfer reactions. Femtosecond transient absorption spectroscopy was here employed to observe absorption changes in the 400–860 nm spectral window occurring in the 0.1–500 ps timescale upon unselective antenna excitation and selective excitation of the Chl-*d* special pair P_{740} in the RC. A numerical decomposition of the absorption changes, including principal component analysis, allowed the identification of $P_{740}^{(+)}Chl_{d2}^{(-)}$ as the primary charge separated state and $P_{740}^{(+)}Pheo_{a3}^{(-)}$ as the successive, secondary, radical pair. A remarkable feature of the electron transfer reaction between Chl_{d2} and $Pheo_{a3}$ is the fast, kinetically unresolved, equilibrium with an estimated ratio of 1:3. The energy level of the stabilised ion-radical state $P_{740}^{(+)}Pheo_{a3}^{(-)}$ was determined to be ~60 meV below that of the RC excited state. In this regard, the energetics and the structural implications of the presence of Pheo-*a* in the electron transfer chain of PSI from *A. marina* are discussed, also in comparison with those of the most diffused Chl-*a* binding RC.

1. Introduction

The two macromolecular chromophore-protein complexes, known as Photosystem II (PSII) and Photosystem I (PSI), are the primary sites of light energy conversion in oxygenic photosynthesis. Whereas the donor side of PSII operates, from a biological perspective, under conditions of extremely high oxidative potential necessary for water photolysis (> + 1 V vs NHE), that of PSI operates at very low redox potential (< −1 V vs NHE) instead [1]. The core complexes of PSI and PSII are generally well conserved throughout evolution and, in both, Chlorophyll (Chl) *a* represents, almost ubiquitously, the main pigment active in light harvesting as well as in primary photochemical electron transfer reactions, that occur in a functionally specialized compartment of the core complex known as the reaction centre (RC). The redox-active cofactors in the RC from the high-resolution structural PSI model of the cyanobacterium *Thermosynechococcus elongatus* [2] are shown in Fig. 1A. This general view has become under scrutiny upon the discovery of oxygenic phototrophs which can replace, to different extents, Chl-*a* with other long

* Correspondence to: S. Santabarbara, Istituto di Biologia e Biotecnologia Agraria, Consiglio Nazionale delle Ricerche, Via Bassini 15a, 20133 Milano, Italy.
** Correspondence to: D. A. Cherepanov, N.N. Semenov Federal Research Center for Chemical Physics, Russian Academy of Sciences, Kosygina Street 1, 119991 Moscow, Russia.
E-mail addresses: stefano.santabarbara@cnr.it (S. Santabarbara), tscherepanov@gmail.com (D.A. Cherepanov).

https://doi.org/10.1016/j.bbabio.2023.148984
Received 7 February 2023; Received in revised form 4 May 2023; Accepted 9 May 2023
Available online 13 May 2023

wavelength, and hence low-energy, Chl molecules (Chl-*d* and -*f*) in the core complexes of both photosystems (e.g. [3–9]). The cyanobacterium *Acaryochloris marina* was the first-discovered organism performing oxygenic photosynthesis in which the otherwise ubiquitous Chl-*a* chromophore is almost completely replaced by Chl-*d* [4,10]. The main electronic transition of Chl-*d* is shifted by about 30 nm towards lower energies with respect to Chl-*a* both in organic solvents [11–13] and in the photosystems' protein environment [10,14]. In the isolated PSI of *A. marina*, the long-lived electron donor displays a main bleaching at 735–740 nm (P_{740}) [15], which is 40 nm red-shifted as compared with the canonical P_{700} of Chl-*a* binding PSI, demonstrating that Chl-*d* can replace Chl-*a* as an electron transfer cofactor in the RC. The assignment of P_{740} to Chl-*d* was confirmed also by hyperfine resolved electron paramagnetic resonance [16] as well as infrared spectroscopy [17]. The red-shift of the P_{740} main absorption band corresponds to an energy lowering of ~90 meV in comparison with P_{700}, assuming that charge separation is initiated from the excited state of this electron donor. Yet, the oxidation midpoint redox potential of P_{740}/P_{740}^{+} falls in the +(425–450) mV range [18–20], hence very close to the midpoint potential of +(430–460) mV measured for canonical P_{700}/P_{700}^{+} pairs in Chl-*a* containing PSI [21].

The PSI of *A. marina* coordinates 1–2 Chl-*a* molecules per core complex [23,24], arguing for possible functional roles of this molecule in photochemical or electron transfer processes. Based on transient absorption (TA) measurements it was proposed that these Chl-*a* molecule (s) acted as the electron acceptor, corresponding to A_0 (also called Chl3 or eC3) in canonical PSI [25]. However, recent structural investigations [22,26] demonstrated that the cofactors in the eC3 positions are not Chl-*a*, rather pheophytin (Pheo) *a,* the Chl-*a* free base (Fig. 1B and C). Although, Pheo-*a* is a common electron acceptor in Type II reaction centres, like PSII and purple bacteria RC, its occurrence in Type I RC, like PSI, is unprecedented.

Due to limited resolution of the structural model, it was not possible to unambiguously assign the chromophores in the so-called Chl2 (eC2) positions, located between P_{740} and eC3, to either Chl-*d* or Chl-*a*. The chlorophyll in the eC2 position is the structural analogue of the accessory bacteriochlorophyll in the bacterial RC, where this pigment acts as the primary electron acceptor [27]. Yet, the functional role of eC2 Chl in PSI is more controversial as it has been suggested to operate as the primary electron acceptor, in analogy with the purple bacterial RC, being part of a functional dimer comprising the eC2-eC3 Chls, corresponding to the functional A_0 acceptor [28–33], but even possibly to act as the primary electron donor(s) [34,35]. Irrespectively of the exact role of the eC2 cofactor, which will be discussed in further detail based on the results obtained in this investigation, it is certain that it plays an important role in PSI photochemical activity. Thus, since the exact chemical nature of the eC2 cofactor in *A. marina* PSI remains to be fully established, a possible role for Chl-*a* in primary photochemistry in this photosystem remains an open question.

Irrespectively of the exact sequence of events and the specific cofactors involved in primary reactions in Chl-*a* containing PSI, which are still a matter of controversy (e.g. [28,29,34–36]), it is yet to be expected that some significant reduction of the driving force associated to light-induced electron transfer occurs in the PSI of *A. marina*. The predicted high reduction potential of Pheo-*a* [11] might act in this direction, thus determining a large change in the photochemical and charge stabilisation reactions energetics. The presence of Pheo-*a* at the eC3 position ($Pheo_{a3}$) shall also influence the successive reduction of phylloquinone A_1, for which a decrease in driving force is predictable. It has however been reported that ultrafast transient absorption (TA) changes of the PSI from *A. marina* are dominated by lifetimes components of about 0.5, 4.5 and 55 ps, for unselective excitation in the main absorption band [25],

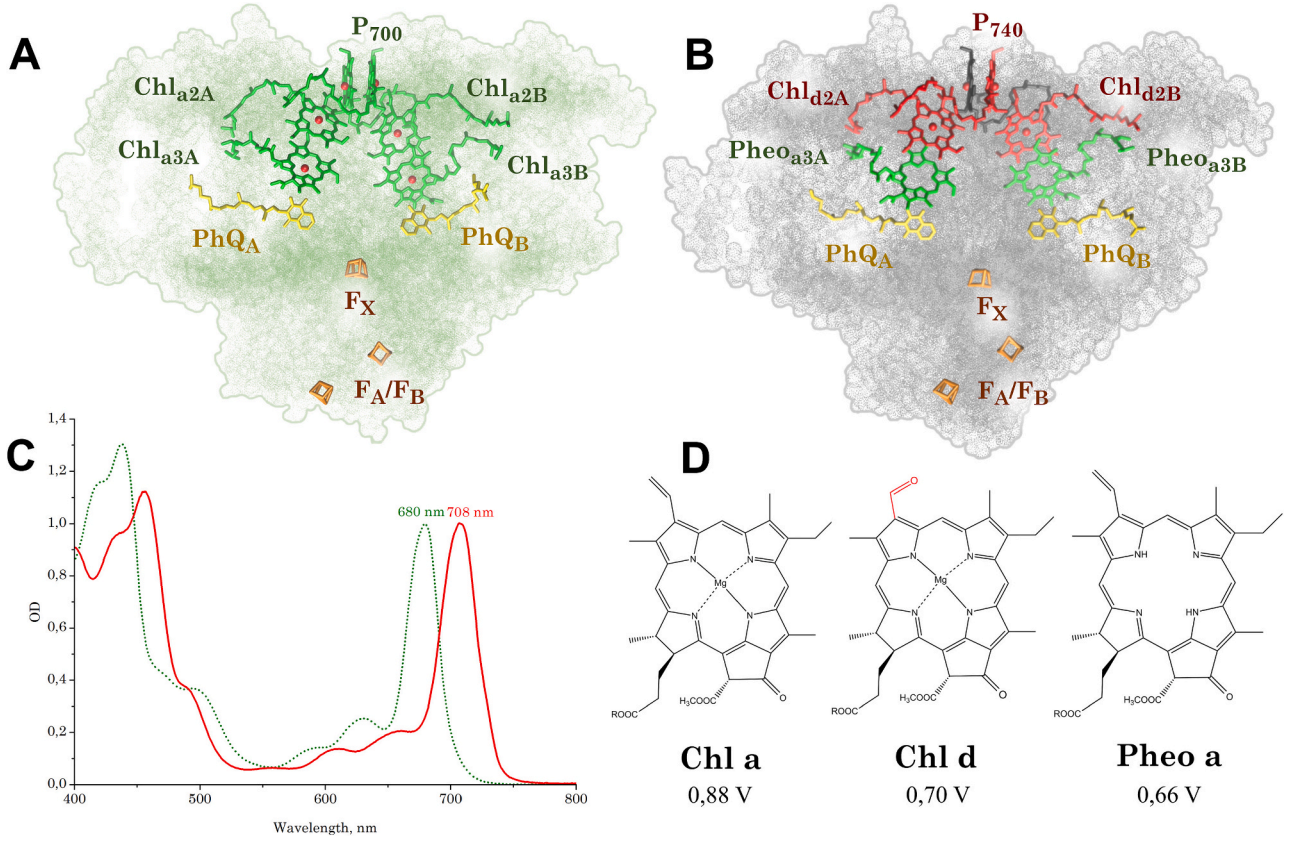

Fig. 1. Electron transfer cofactors of the PSI complexes from *T. elongatus* [2] (**A**) and *A. marina* [22] (**B**). The absorption spectrum of the PSI from *A. marina* is red-shifted when compared to the absorption spectrum of the canonical PSI (**C**) due to the presence of Chl-*d* instead of Chl-*a* in the light-harvesting antenna (**D**). The reaction centre of PSI from *A. marina* harbours four Chl-*d* and two Pheo-*a* molecules in places of six Chl-*a* molecules in the PSI from *T. elongatus*.

and similarly for excitation in the red edge at 720 nm (4 and 36 ps) [37]. These values are relatively similar to the lifetimes retrieved in other cyanobacterial PSI complexes either by fluorescence lifetime (e.g. [38–41]) or TA measurements [29,30,42–45]. Hence, it appears that some energetic reconfiguration occurs in *A. marina* PSI, allowing the system to operate with similar kinetics and yields as canonical PSI.

The kinetics of charge recombination either from the terminal iron-sulphur clusters $F_{A/B}$ (40–60 ms) and F_X (1.5–2 ms) at room temperature [15,20], or from the quinone acceptor A_1 both at room (190 μs) and cryogenic temperatures (150 μs, [20]), are comparable to those reported for canonical Chl-*a* binding PSI (e.g. [46] for a review). A somewhat larger difference was reported for the A_1^- oxidation by F_X, in *A. marina*, since the dominant lifetimes were estimated as 356 ns and 88 ns with respect to 285 ns and 18 ns in the model cyanobacterium *Synechocystis* sp. PCC 6803 investigated under the same conditions [47]. Considering that both structural [22,26] and functional spectroscopic investigations [48] indicate a close similarity of the overall cofactor arrangements between *A. marina* and canonical PSI, the differences in A_1^- oxidation point towards some reconfigurations of the redox properties of either A_1 or the acceptor F_X in *A. marina*. Yet, the similarity of recombination kinetics indicates that the overall energy difference between the acceptor and the donor side of the Chl-*a* and Chl-*d* binding photosystem is maintained, arguing in favour of the main energetic compensation for the loss in photon energy of P_{740}* occurring at the level of primary and charge stabilisation reaction, likely involving the unusual Pheo-*a* acceptor at the eC3 position.

In order to further understand the molecular mechanism of these reactions in this unique photosystem, the isolated pigment-protein complex was studied by TA with high-spectral and-temporal resolution (100 fs), upon either unselective (630 nm) or preferential excitation of low energy Chl-*d* forms and the RC cofactors, in the near-infrared (740 nm).

2. Materials and methods

2.1. Sample preparation

A. marina cells were cultivated at 21 °C in a modified BG11 medium in artificial sea-water (SW-BG11), under continuous illumination (35 μmoles of photon m^{-2} s^{-1}) provided by incandescent lamps. Thylakoid membranes (TM) were purified from freshly harvested cells suspended in 50 mM HEPES in the presence of ε-aminocaproic acid and phenylmethanesulfonyl fluoride (PMSF), and broken by glass beads (212–300 μm) in a TissueLyzer (Qiagen) performing 15 circles of cell shaking (15″ at the maximal shaking frequency of 30 Hz) and 3′ cooling on ice between each cycle. Unbroken cells and large debris were removed by centrifugation at 9000 rpm for 5′, and TM were harvested by successive ultracentrifugation at 144000 x*g* and re-suspended in 50 mM Hepes/NaOH buffer (pH 7.5). All procedures were performed at 4 °C and under dim light or darkness.

For PSI isolation, thylakoids were solubilised for 1 h with 1 % *w/v* β-n-dodecylmaltoside in the resuspension buffer at a concentration equivalent to 0.5 mg/ml Chl ($d + a$), in complete darkness and at 4 °C. PS I was separated by centrifugation on sucrose density gradients as previously described [49]. The lowest band corresponding to PSI was harvested, dialyzed, washed, concentrated (50 kDa cut-off), frozen in liquid nitrogen and stored at −80 °C until use. Further detail on the methods is provided in the Supplementary Information.

2.2. Ultrafast spectroscopy

Time-resolved difference absorption spectra ΔA(λ,t) were measured by a pump–probe method using the previously described set-up [30]. In brief, the sample was pumped either at 630 or 740 nm (~38 nm FWHM) from the compressed (23 fs) output of an optical parametric amplifier, attenuated to 25–80 nJ/pulse. The probe was provided by broadband supercontinuum pulses, at magic (54.7°) polarisation with respect to the pump pulse. Absorption difference spectra in the 400–900 nm range were collected by a CCD camera (Roper Scientific SPEC-10) coupled to a polychromator (Acton SP-300). The experiments were carried out at 6 °C in a 0.5-mm flow optical cell with optical windows of 0.1-mm thickness (10 O.D. cm^{-1}). The circulation rate in the flow cell (9 ml min^{-1}) was fast enough to avoid multiple excitations of the same sample volume. Spectra were corrected by group delay dispersion as described previously [50,51].

2.3. Data analysis

The TA changes were analysed by three different numerical approaches that approximate the spectral-temporal matrix $\Delta A(\lambda, t)$ in terms of:

(i) A linear combination of discrete exponential decay functions $\sum_i D_i(\lambda) exp(-t/\tau_i)$ with globally constrained lifetimes, τ_i, and independent amplitudes giving the Decay Associated Spectra (DAS), $D_i(\lambda)$ (see section S2.1 of Supplementary Information for details).

(ii) Continuous integral transform $\int \rho(\lambda, \tau) e^{-t/\tau} d\tau$ allowing to remove the constraints imposed by the global discrete decomposition. In brief, the continuous spectral-lifetime distribution $\rho(\lambda, \tau)$ was calculated independently at each wavelength λ by the inverse Laplace transform using a modified version of the CONTIN algorithm [52]. To obtain quasi-continuous behaviour of lifetime density maps (LDM) against λ, an additional regularization was applied to the standard Tikhonov–Phillips regularising parameter α (see S2.2 for details).

(iii) Principal components. The principal component analysis (PCA) [53,54] is a fully model-independent method, which does not require any a priori analytical description of the kinetics. The matrix $\Delta A(\lambda, t)$ was expanded in a series $\sum_j S_j(\lambda) P_j(t)$, where $S_j(\lambda)$ is the spectrum of the j^{th} principal component and $P_j(t)$ is its time-dependent contribution (score). The first principal component ($j = 1$) accounts for the highest possible variation of $\Delta A(\lambda, t)$, the second for the largest remaining variation, and so on until the residual time-independent component is reached (see S2.3 for details).

3. Results

3.1. Transient absorption changes of PSI from A. marina

Femtosecond pump-probe laser spectroscopy was used to study ultrafast absorption changes related to excitation energy and electron transfer processes in the PSI complexes isolated from *A. marina*. In this technique, an ultrashort narrow-beam pulse (pump) is used to excite the sample, and a weaker broad probe pulse is used to monitor the photo-induced difference absorption changes obtained by subtracting the absorption of the non-irradiated sample measured in the same cell. Absorption changes of PSI were acquired in the 400–860 nm window in the 0.1–500 ps timescale upon unselective excitation at 630 nm (Fig. 2A) or selective excitation at 740 nm (Fig. 2B) in the far-red edge of the Chl-*d* Q_Y band (Fig. S1).

The absorption **characteristics** of the samples did not change after measurements within 20 min and also when the excitation energy varied in the range of 30–80 nJ (Fig. S2). The respective spectral-temporal matrices $\Delta A(\lambda,t)$ (Fig. S3) were analysed in terms of discrete exponentials (Eq. S1), and at least five exponentially decaying components were required to realistically describe the experimental data (Fig. S4). When the spectral dynamics were decomposed into six components, the uncertainties of their lifetimes (Eq. S5) became too large, so for an appropriate description of the overall TA dynamics upon PSI excitation both at 630 and 740 nm, five global exponential components were employed (Table 1, Figs. 3 and 4). Alternatively, the continuous lifetime distribution maps (LDM, see S2.2 for details) were calculated in

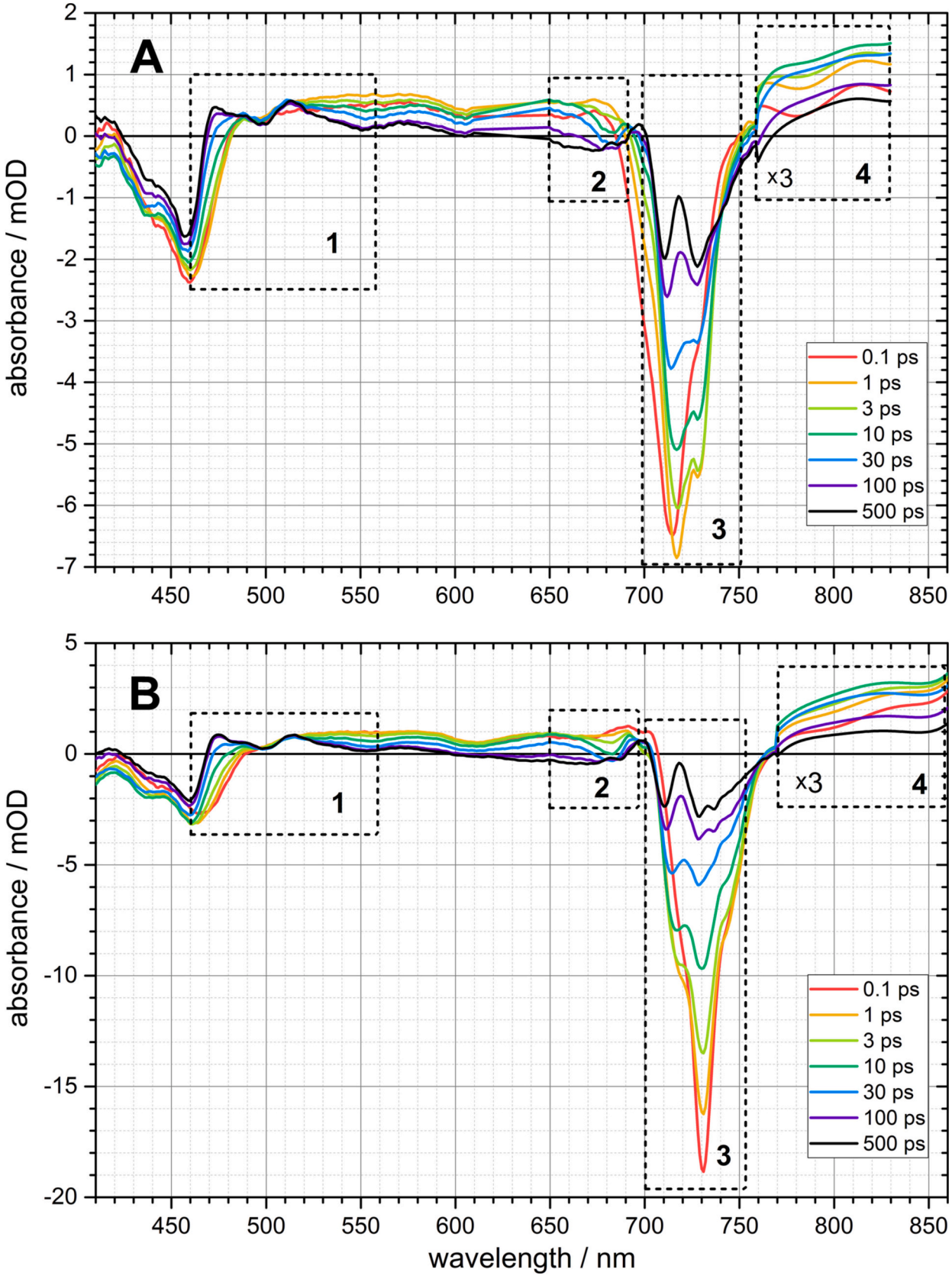

Fig. 2. TA spectra of *A. marina* PSI at selected time delays upon excitation at 630 nm (**A**) and 740 nm (**B**). The boxes indicate the spectral regions which were subjected to PCA analysis (see Section 3.2 for details).

Table 1
Lifetimes derived from global analysis of *A. marina* PSI transient absorption.

Pump	τ_1 (ps)	τ_2 (ps)	τ_3 (ps)	τ_4 (ps)	τ_5 (ps)
630 nm	0.15 (±0.04)	0.5 (±0.1)	2.0 (±0.4)	17 (±3)	71 (±9)
740 nm	0.15 ± 0.02)	1.3 (±0.1)	6.8 (±1.6)	28 (±7)	130 (±64)

accordance with Eq. S6 (Fig. 5).

The lifetimes and related Decay Associated Spectra (DAS, Figs. 3 and 4) obtained by global fitting agree closely to the main lifetime clusters and spectral features observed in the LDMs (marked by arrows in Fig. 5). Yet the information concerning kinetic dispersion are lost in global analysis, hence we focus on the analysis of the LDMs.

Upon non-selective excitation at 630 nm, the LDM revealed a significant kinetic dispersion in the Q_Y region of 690–730 nm (Fig. 5A), being only roughly approximated by the five discrete lifetimes of the DAS decomposition (Fig. 3, Table 1). In the fastest lifetime clusters τ_1 (0.1–0.2 ps) and τ_2 (0.4–0.6 ps), energy transfer processes prevail. A broad area of absorption increase at 680–710 nm (shown in red) and a narrow bleaching spot at 725–735 nm (shown in blue) are the most

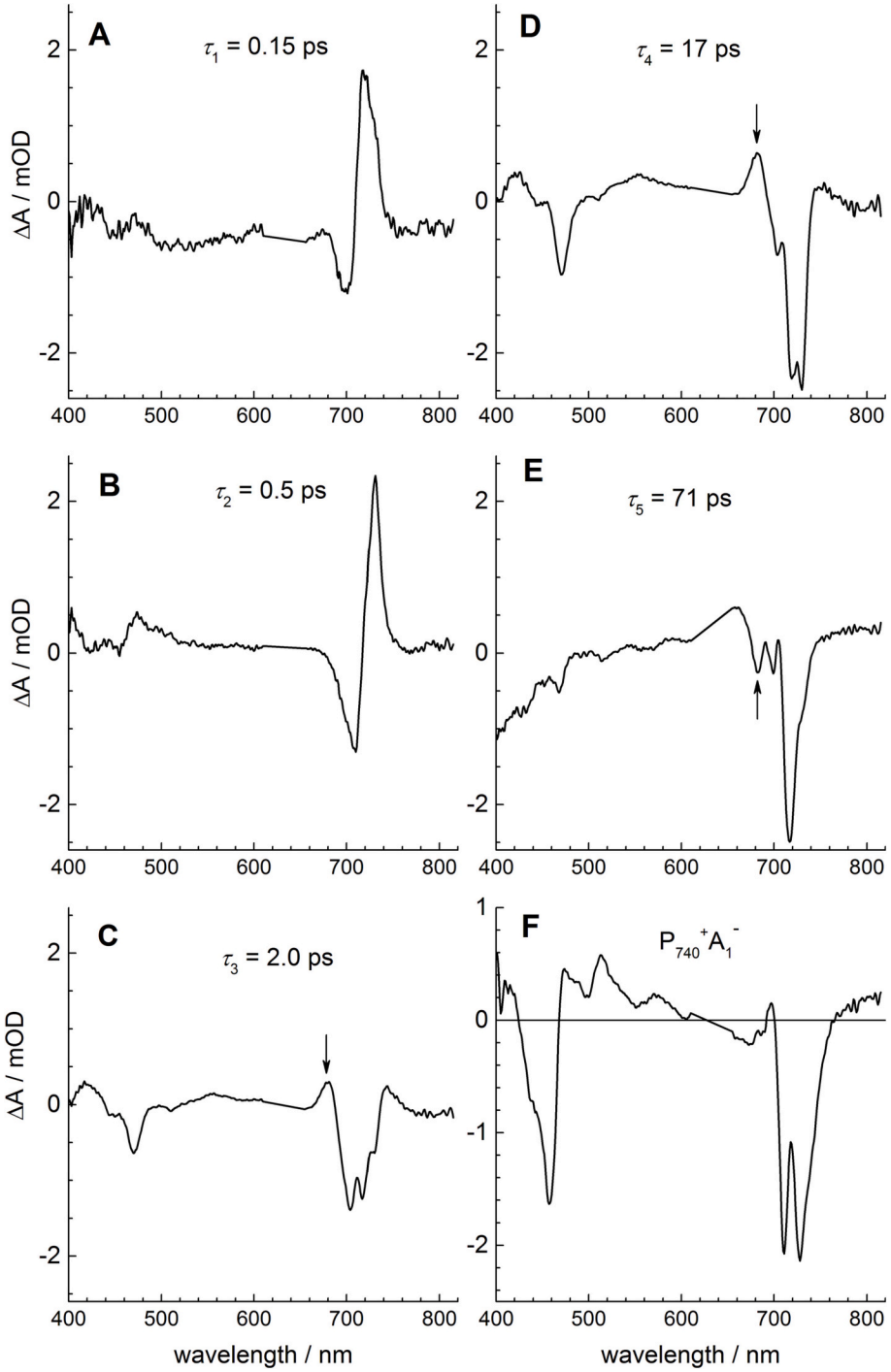

Fig. 3. Decay-Associated Spectra of the PSI from *A. marina*. The decay times: 0.15 ps (**A**), 0.5 ps (**B**), 2.0 ps (**C**), 17 ps (**D**), and 71 ps (**E**). The final spectrum at delay of 500 ps (**F**) corresponds to the secondary radical pair $P_{740}^+A_1^-$. Down- and up-pointing arrows mark the bleach and recovery bands of Pheo-*a* absorption at 682 nm. Excitation at 630 nm (duration 23 fs, FWHM 38 nm, energy 50 nJ).

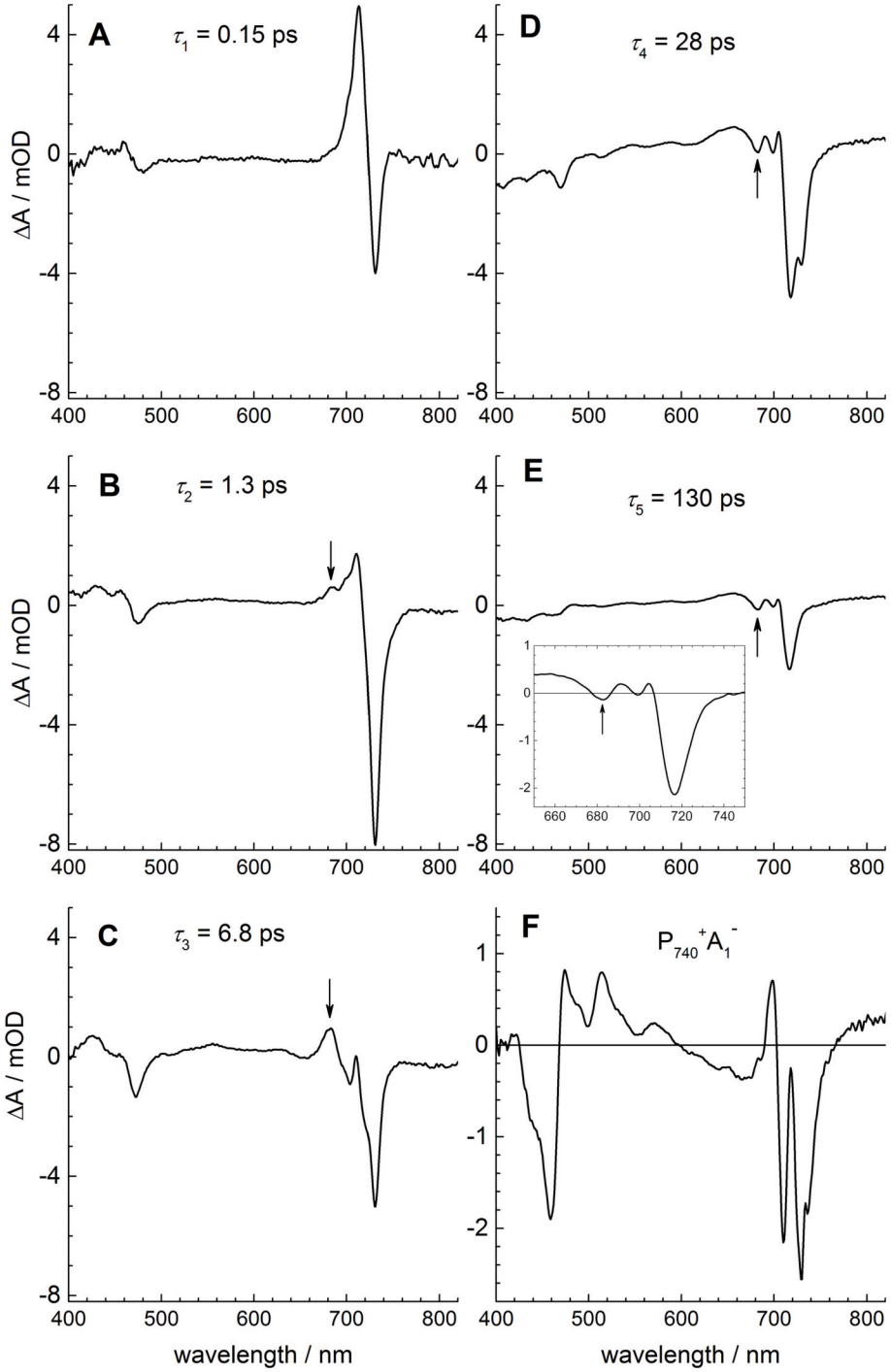

Fig. 4. Decay-Associated Spectra of the PSI from *A. marina*. The decay times: 0.15 ps (**A**), 1.3 ps (**B**), 6.8 ps (**C**), 28 ps (**D**), and 130 ps (**E**). The final spectrum at delay of 500 ps (**F**) corresponds to the secondary ion-radical pair $P_{740}^{+}A_1^{-}$. Down- and up-pointing arrows mark the bleach and recovery bands of Pheo-*a* absorption at 682 nm. Excitation at 740 nm (duration 23 fs, FWHM 38 nm, energy 80 nJ).

prominent features in this time range. These processes may be attributed, dominantly, to downhill energy transfer from the bulk of the photosystem's antenna to a long-wavelength Chl-*d* (LWC) pool centred at ~730 nm.

The cluster τ_3 (1.6–2.4 ps) includes a broad absorption decrease at 420 nm, a sharp peak of absorption growth at 470 nm, a broad structured increase at 700–730 nm in the Q_Y region, and the development of a sharp minor bleaching at 682 nm (denoted by down-pointing arrow in Fig. 3C, which shows the DAS corresponding to the equivalent lifetime cluster). These features apparently are related to the initial phase of energy trapping due to the formation of ion-radical pairs: the absorption increase at 470 nm is a distinctive marker of the oxidized P_{740} [20], and the ground state bleaching (GSB) at 682 nm corresponds to the expected absorption of Pheo-*a* recently identified in the eC3/A_0 position [22,26]. The prevailing absorption recovery, with the main bands centred at 704 and 718 nm in the Q_Y region, can be explained by the energy transfer from the antenna to the RC and by the disappearance of both the GSB and stimulated emission (SE) as a result of charge separation (the amplitude of SE is approximately equal to the GSB contribution [13,55]). The lifetime cluster τ_4 (14–20 ps) also shows the development

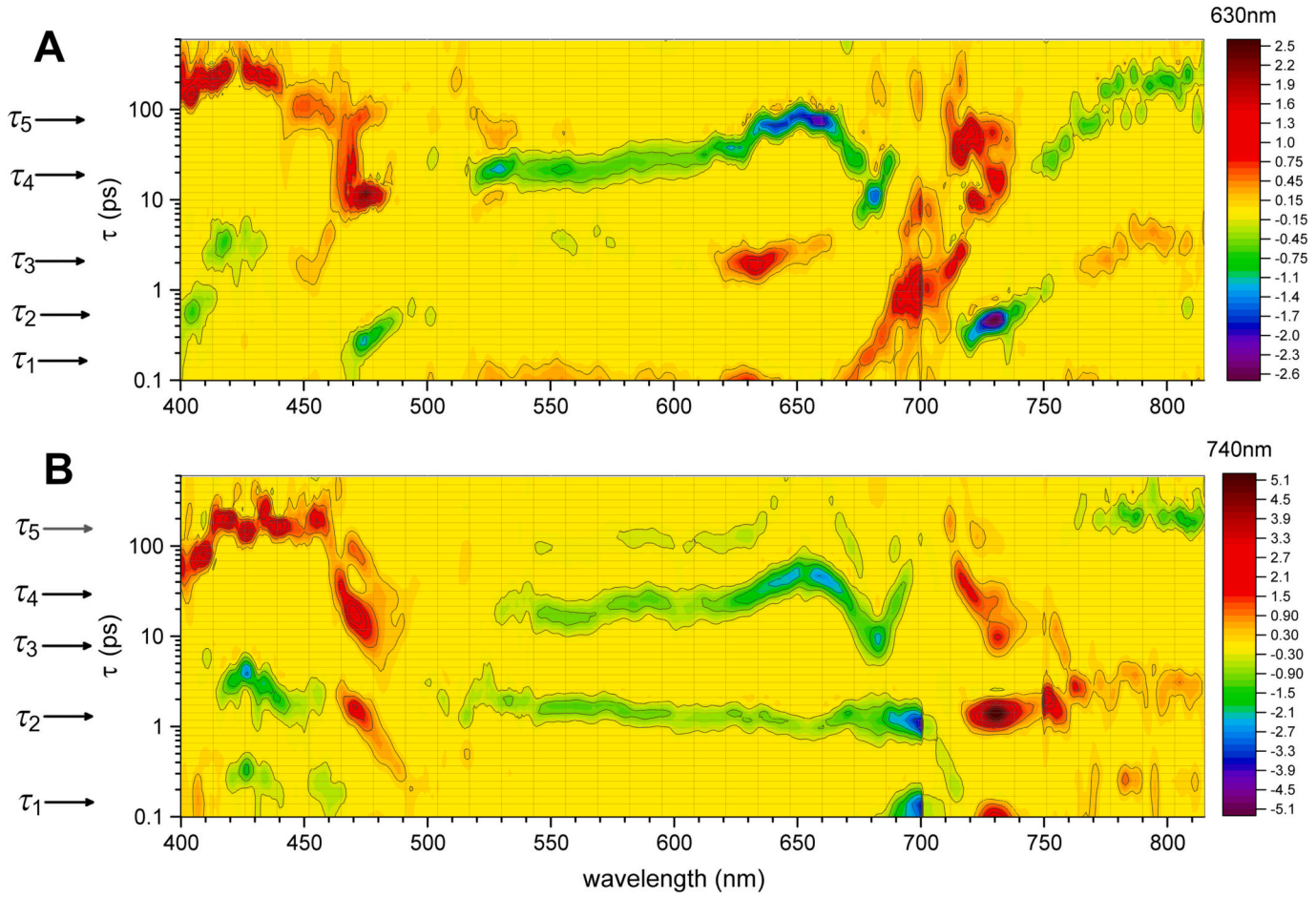

Fig. 5. Lifetime distribution analysis, presented as density maps (LDM), of the TA kinetic in *A. marina* PSI excited at 630 nm (**A**) and 740 nm (**B**). The LDM amplitudes in the 700–750 nm were damped by a factor of 5. The lifetimes retrieved from the global analysis and the associated DAS decomposition (Table 1) are indicated by the arrows next to the lifetime axis.

of GSB at 682 nm, but the excitation donors in this case comprise chromophores with Q_Y bands peaking at 718 and 730 nm. Moreover, the absorption changes in this lifetime cluster are larger with respect to those dominating the cluster τ_3. These spectral differences are also clearly appreciated by comparing the DAS in Fig. 3C and Fig. 3D. The broad absorption decrease at 520–620 nm originates due to trapping of the Chl-*d* excited S_1 state (Fig. S1C), monitored over its broad excited state absorption (ESA) band [13].

The slowest cluster τ_5 (62–80 ps) has a complicated pattern that includes a broad absorption recovery in the Soret band at 400–480 nm (with only a minor contribution of the 470 nm peak), a recovery of the sharp bleach peak at 718 nm with a modest shoulder at 730 nm, that is also accompanied by the recovery of the bleach peak at 682 nm (up-pointing arrow in Fig. 3E). The cluster demonstrates also a small-scale broad absorption decrease at 630–660 nm and above 760 nm. These processes appear to correlate with the kinetics clustered around 2 ps in Fig. 5A that have similar spectral signature, but opposite sign. This cluster could be associated to oxidation of Chl-*d* and Pheo-*a* ions [56] because the excited Chl-*d* (Fig. S1C) has only very weak extinction in the spectral range above 800 nm. The residual positive absorption in the far-red region observed at the longest time delay of 500 ps (Fig. 2) should be assigned to the P^+_{740} cation [20].

Excitation at 740 nm affected selectively an ensemble of ~25 Chl-*d* molecules in the far-red range of 710–740 nm (Fig. S5 and S6); as a result, the absorption dynamics at $\Delta t \leq 10$ ps differed from the non-selective excitation (Fig. S3). An ultrafast 0.15 ps (τ_1) cluster depicts uphill energy redistribution in the antenna Fig. 5B. The excited state redistribution is also apparent in the shape of fastest resolved DAS shown in Fig. 4A. The successive lifetime cluster (τ_2) centred at 1–2 ps, besides uphill energy redistribution, demonstrates also features of ion-radical pairs formation: absorption increase at 470 nm (P^+_{740}), rise of the bleaching at 682 nm (Pheo-*a*), and absorption decrease at 520–650 nm (ESA) due to trapping of the excited Chl-*d*. Under selective excitation at 740 nm, charge separation in RC, monitored by the absorption band at 470 nm (cation P_{740}) and the bleaching band at 682 nm (anion Pheo-*a*), occurs predominantly in the time cluster of 6–10 ps (τ_3), the main donor of excitation is the Chl-*d* pool with a maximum at 730 nm and to a lower extent at 720 nm. Formation of the P^+_{740} cation in a smaller amount is also observed in the time interval of 20–40 ps (τ_4), however, in contrast to the TA dynamics in this time range upon the non-selective excitation, some recovery of the bleach peak at 682 nm is observed (up-pointing arrow in Fig. 4D), most likely as a result of electron transfer to the next acceptor in the electron transfer chain, the phylloquinone A_1.

The slowest lifetime cluster τ_5 in the 65–200 ps lifetime window resembles the analogous cluster obtained for the nonselective excitation at 630 nm, although with a higher dispersion of the lifetime distribution. The DAS component with the lifetime of 130 ps obtained by the discrete exponential decomposition shows that the absorption changes in the Q_Y region are dominated by a broad unstructured band with a maximum at 716 nm, the amplitude of which is approximately four times the amplitude of the Pheo-*a* band bleach at 682 nm (inset in Fig. 4E). This cluster therefore could be associated to oxidation of Chl-*d* and Pheo-*a* anions, and also to the disappearance of GSB and SE bands of excited Chl-*d* in the antenna.

3.2. Principal component analysis of absorption changes

In order to assess by a model-independent analysis the spectral characteristics of the largely dispersed kinetics, and focusing particularly on resolving the cofactors participating in primary photochemical and successive electron transfer events, the spectral-temporal matriceswere analysed by the PCA method [53,54] in four spectral windows: i) $460 \leq \lambda_1 \leq 560$ (region 1 in Fig. 2) represents a specific marker of P_{740} oxidation [20]); ii) $650 \leq \lambda_2 \leq 690$ (region 2) serves as a marker of Pheo-*a* reduction [57,58]; iii) $700 \leq \lambda_3 \leq 750$ (region 3) contains contributions from SE and GSB of exited Chl-*d* both of the antenna and RC; iv) $760 \leq \lambda_4 \leq 860$ (region 4) accounts predominantly for the Chl-*d* and Pheo-*a* anions [56] as well as the P_{740}^{+} cation [20] absorption, since the excited Chl-*d* has a very weak infra-red absorption ([13] and Fig. S1C). Each principal component *i* is a product of its spectral form $S_i(\lambda)$ and its score $P_i(t)$; the results of PCA decomposition of the four spectral regions are presented in Fig. 6 and Figs. S7-S9, the percentage of the total variance explained by each principal component (PC) is summarized in Table S2.

Fig. 6 shows the principal components in the λ_1 and λ_2 regions, which correspond nicely to the expected difference spectra associated to P_{740} oxidation (Fig. 6A) and Pheo-*a* reduction (Fig. 6B). To obtain actual concentrations (molar fractions), the PC need to be scaled to some measurable quantities. The fractional dynamics of P_{740} cation were assessed assuming that the concentration of P_{740}^{+} per RC is zero at $t = 0.1$ ps and that it reaches unity at $t = 500$ ps (see Fig. S10 and Suppl. 4.2). The transient Pheo-*a* reduction at the eC3 position ($Pheo_{a3}^{-}$) was estimated from the known extinction of Pheo-*a* in the Q_Y band (Fig. S11). The dynamics of P_{740}^{+} and $Pheo_{a3}^{-}$, in mole/RC units, are shown in Fig. 6D and E for the experiments performed with 630 nm and 740 nm excitation, respectively. The third $700 \leq \lambda_3 \leq 750$ region is more spectrally congested as it includes contributions of a large number of excited Chl *d* states in the antenna, as well as spectral changes due to photochemically generated radical pair states in the RC. The first two principal components $S_j(\lambda)$ spectra and relative contributions $P_j(t)$ in the λ_3 window are shown in Fig. S9. Figs. 6C and F show spectra and score factors for the λ_4 region, where only relative scores for anion Chl-*d* and Pheo-*a* states were determined. Nonetheless, the infra-red region ($760 \leq \lambda_4 \leq 860$) is of particular interest because the TA dynamics in this spectral window contains information about the eventual appearance of photochemically generated ionic states, whereas Chl-*d* excited state contributions are virtually negligible. Thus, radical pairs can be observed almost selectively in the λ_4 region. The kinetic profile of the major PC in this region is similar to the one assignable to $Pheo_{a3}$ reduction, deduced

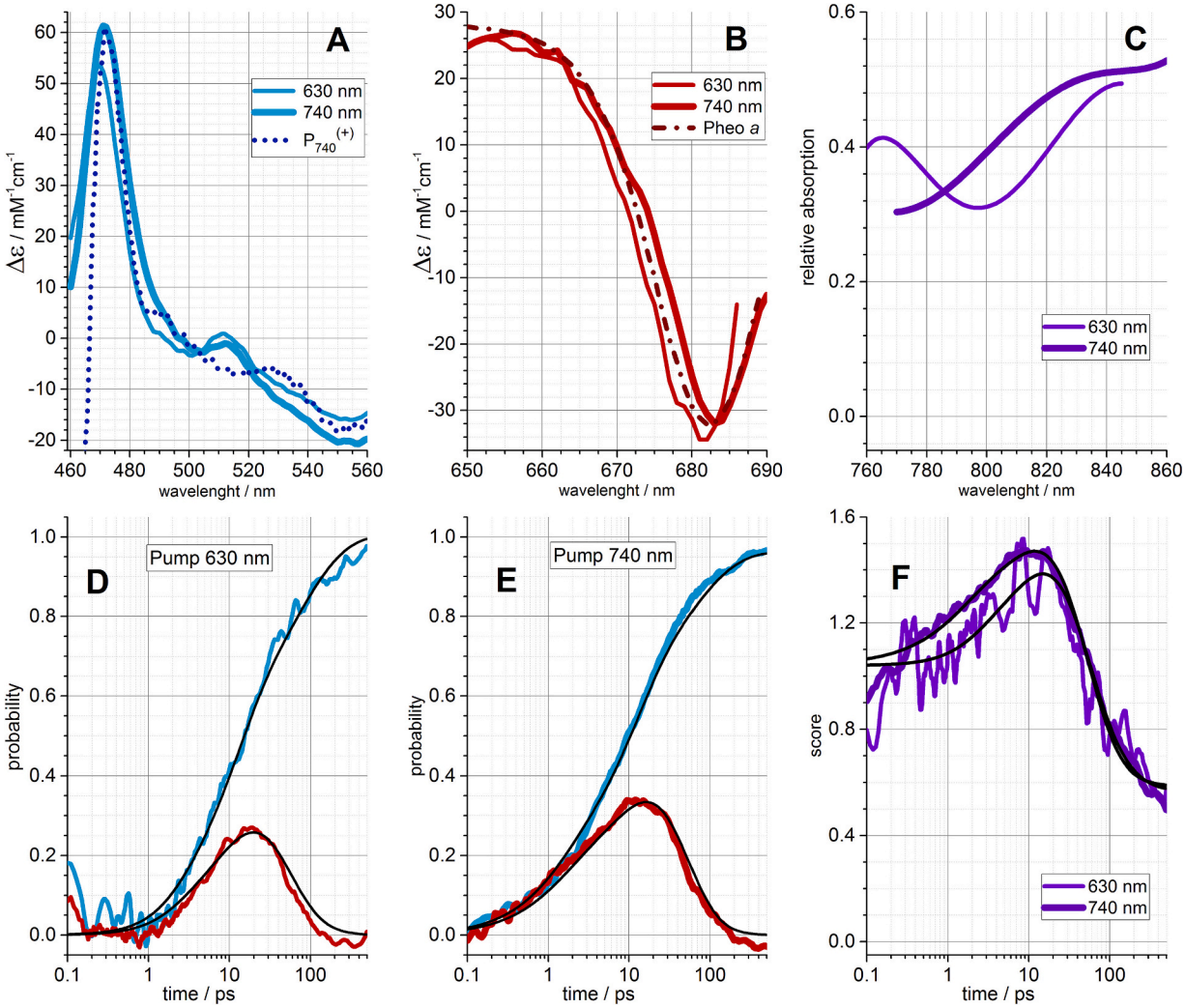

Fig. 6. The partial spectra $\varepsilon_j(\lambda)$ (**A, B, C**) and relative contributions $P_j(t)$ (**D, E, F**) of the principal components characterising the transient absorption of P_{740}^{+} (cyan), reduced Pheo-*a* (red), and anion states of Chl-*d* and Pheo-*a* (violet) in *A. marina* PSI excited at 630 nm (thin lines) and 740 nm (thick lines). The difference absorption spectrum of P_{740}^{+}-P_{740} (dots) [20] and the flipped spectrum of Pheo-*a* in acetone (dash-dots) [59] are superimposed with the partial spectra in (**A**) and (**B**). Thin black lines show the results of kinetic modelling with the parameters from Table 2. (For interpretation of the references to colour in this figure legend, the reader is referred to the web version of this article.)

from the analysis of the marker region λ_2. This indicates that contributions from Chl-*d* anions are kinetically indistinguishable/or substantially overlapped to those of Pheo-*a* anions and that therefore these cofactors seem to have almost concerted oxidation/reduction dynamics.

Fig. 6 clearly shows that the oxidation of P_{740} and reduction of $Pheo_{a3}$ appear to start synchronously, either at a delay of ~2 ps (excitation at 630 nm, Fig. 6D) or at ~0.2 ps (excitation at 740 nm, Fig. 6E) from initial excitation. At delays up to 10 ps the relative contribution of $Pheo_{a3}^-$ is lower than the contribution of P_{740}^+, which means that the amount of the formed $Pheo_{a3}^-$ is proportionally lower as compared to the P_{740}^+. The difference in the contributions indicates the presence of another anion, which can then be attributed to Chl-*d* at the eC2 position (Chl_{d2}^-).

These results allow us to conclude that in *A. marina* PSI the primary electron donor is P_{740} while Chl_{d2} is the primary electron acceptor, because if Chl_{d2} would function as the primary donor and $Pheo_{a3}$ is the

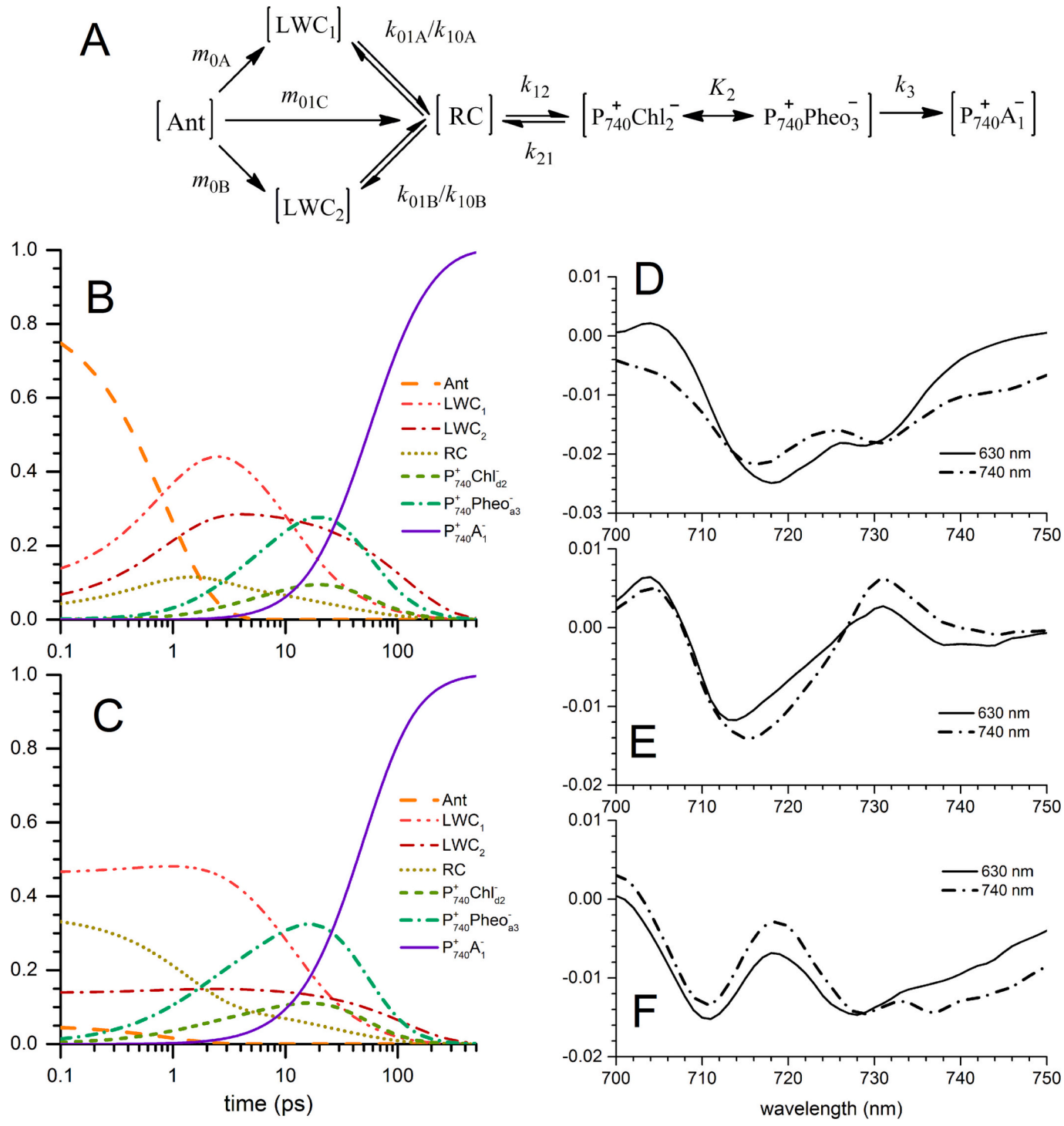

Fig. 7. Kinetic modelling of energy and electron transfer in PSI from *A. marina*. In the kinetic scheme (**A**) brackets indicate separate kinetic compartments. Population dynamics of the electronic states described in Panel A for unselective (**B**) and far-red (**C**) excitation conditions. The difference spectra of exited RC (**D**), the primary $P_{740}^+Chl_{d2}^-$ (**E**) and the secondary $P_{740}^+A_1^-$ (**F**) radical pairs calculated by the PCA decomposition of TA dynamics upon excitation at 630 nm (solid) and 740 nm (dash-dotted). The rate and equilibrium constants are listed in Table 2.

primary acceptor, the concentration of $Pheo_{a3}^{-}$ would be higher than the concentration of P_{740}^{+} in the considered time range. Thus, Figs. 6D and E show unambiguously that (i) the primary electron donor is P_{740} and (ii) the redistribution of electrons between Chl_{d2} and $Pheo_{a3}$ proceeds faster than ~0.2 ps, explaining their overlapped dynamics in the near infrared (λ_4) window.

3.3. Kinetic modelling of absorption changes

The data obtained by the PCA approach were used to develop a minimum kinetic model consistent with the structural data [22,26], which includes seven electronic states and six kinetic compartments (Fig. 7A). The model considers three excited state compartments of the antenna: one accounts for the short-wavelength (*Ant*) and two for long-wavelength (LWC_1 and LWC_2) Chl-*d* spectral forms. The energy migration from *Ant* to the low-energy states LWC_1, LWC_2 and *RC* is described by the rate constants m_{0A}, m_{0B} and m_{0C}, respectively. Because LWC_1 and LWC_2 are almost isoenergetic with *RC*, the reversible transitions between them are described by the rate constants k_{01A}/k_{10A} and k_{01B}/k_{10B}, respectively.

Three radical pair states are also considered,$P_{740}^{+}Chl_{d2}^{-}$, $P_{740}^{+}Pheo_{a3}^{-}$ and $P_{740}^{+}A_1^{-}$. Photochemical formation of the primary radical pair$P_{740}^{+}Chl_{d2}^{-}$ from *RC** is accounted by the rates k_{12} and k_{21}.The population of the successive radical pair, $P_{740}^{+}Pheo_{a3}^{-}$, is considered as being in a fast equilibrium with $P_{740}^{+}Chl_{d2}^{-}$, so that the two radical pairs are combined in one kinetic compartment with the internal equilibrium constant K_2. The population of the long-lived $P_{740}^{+}A_1^{-}$state is described by the rate constant k_3. For the selective excitation conditions (740 nm), the initial excitation distribution between the 75 Chl-*d* molecules of PSI was determined by the overlap of their Q_Y absorption bands and the 740 nm pump pulse spectrum (Fig. S6), whereas for the unselective conditions (630 nm), the excitation distribution is fundamentally determined by the number of pigments in each antenna compartment.

The parameters of the unified kinetic model were determined by numeric non-linear optimization of PCA components population, $P_j(t)$, in the four spectral regions considered (Table 2). The fitting to the kinetic model, demonstrating a close agreement with the PCA dynamics, are shown in Fig. 6D, E, F and S12. Fig. 7 shows the populations of the kinetic compartments and the difference spectra associated with *RC** together with the $P_{740}^{+}Chl_{d2}^{-}$ and the $P_{740}^{+}A_1^{-}$radical pairs, resulting from PCA decompositions. These spectra are almost independent on the excitation conditions, further supporting the validity of the kinetic model employed. The spectrum of the $P_{740}^{+}Chl_{d2}^{-}$ state (Fig. 7E) shows a dominant bleaching at 716 nm, indicating unambiguously that the cofactor at the eC2 position is a Chl-*d* molecule. It is noticeable that both the equilibrium constants for primary charge separation (k_{12}/k_{21}.) and secondary electron transfer, K_2, are rather low (about 3–4, see Table 2). The implications of these results on the photosystem's energetics are further discussed below.

4. Discussion

4.1. Electronic transitions in the reaction Centre of Photosystem I from Acaryochloris marina

The PSI from *A. marina* harbours a unique complement of cofactors. The low-energy Chl-*d* substitutes Chl-*a* both in the antenna and in the RC, while Pheo-*a* molecules occupy the $eC3_A/eC3_B$ structural positions in the RC [2]. The latter peculiar feature of the *A. marina* PSI has been recently revealed by structural studies [22,26], yet the contribution of these cofactors in primary photochemical and successive charge stabilisation reactions remained unclear. The investigation of ultrafast TA dynamics of the *A. marina* PSI provides a unique opportunity to solve this problem.

The occurrence of Pheo-*a* as an electron transfer cofactor, constitutes an important advantage for the study of the molecular mechanism of photochemical reactions in *A. marina* PSI in comparison to the canonical Chl-*a* binding counterpart. This is because the Q_Y absorption band of Pheo-*a*, being located around 680 nm, serves as a distinct spectral marker. It is clearly separated from spectral changes of Chl-*d*, since the electronic transitions of the latter fall in the 700–740 nm window, both for excitation transfer in the antenna and electron transfer in the RC.

Previous femtosecond measurements of absorption dynamics in the isolated PSI from *A. marina*, induced by excitation at 630 nm, revealed a bleach band at 680 nm developing with a time of ~6 ps and disappearing with a time of ~40 ps, which was attributed to a Chl-*a* molecule functioning as the primary electron acceptor in one of the branches of RC [25]. However, the restrictions of the measurements in time (0.25–300 ps) and spectral range (660–780 nm) did not allow the authors to determine the kinetics of P_{740} oxidation and to identify the sequence of primary charge separation reactions. Here the measurements performed over a wider spectral window (400–860 nm) and upon selective excitation of PSI in the infra-red edge of the Q_Y band, make it possible to compare the kinetics of Pheo-*a* reduction with those of P_{740} oxidation and, in turn, to unambiguously identify the primary and secondary radical pairs in this peculiar PSI system.

The primary charge separated state is identified as $P_{740}^{+}Chl_{d2}^{-}$, where Chl-*d* at the eC2 position acts as the primary electron acceptor. The next radical pair state is assigned to $P_{740}^{+}Pheo_{a3}^{-}$. All spectral changes that could arise from Chl-*a* molecules, are actually associated to the reduction of Pheo-*a* through the formation of $P_{740}^{+}Pheo_{a3}^{-}$. This excludes, to a good level of confidence, any possible involvement of Chl-*a* in either photochemical or ET transfer reactions. The appearance of the Pheo-*a* bleach at 682 nm starts synchronously with the P_{740} oxidation (Fig. 6D and E), which indicates that Chl-*d* in the eC2 position and Pheo-*a* in the eC3 position are in a fast equilibrium. The equilibrium constants $K_1 = k_{12}/k_{21}$ and K_2 associated to the formation of the $P_{740}^{+}Chl_{d2}^{-}$ and the $P_{740}^{+}Pheo_{a3}^{-}$ radical pairs (see Fig. 7A) were estimated to be 3.7 and 3.1, respectively (Table 2), corresponding to a total driving force ($-\Delta G_{RP_2}$) of 63 meV for the population of the stabilised, secondary, radical pair (~2.5 k_BT for $T = 300$ K).

The small magnitude of equilibrium constant K_2 between the

Table 2
Kinetic parameters of energy and electron transfer reactions in PSI from *A. marina*.

	Energy transfer					Charge transfer		
	Branch A		Branch B		Direct	Primary		Secondary
	Ant→LWC_1↔*RC*		*Ant*→LWC_2↔*RC*		*Ant*→*RC*	P_{740} ↔ Chl_{d2} ⇔ $Pheo_{3a}$ → A_1		
	m_{0A}	k_{01A}/k_{10A}	m_{0B}	k_{01B}/k_{10B}	m_{0C}	k_{12}/k_{21}	K_2	k_3
k_f		110	370	8.2	220	560		40
k_r	–	200	–	0	–	150		
K_{eq}	–	0.55	–	–	–	3.7	3.1	–

Initial conditions *Ant*, LWC_1, LWC_2 and *RC* are distributed in proportion 0.84, 0.09, 0.04 and 0.03 (630 nm) and 0.05, 0.46, 0.14 and 0.35 (740 nm). The kinetic constants of forward (k_f) and backward (k_r) reactions are given in ns^{-1}.

$P^+_{740}Chl^-_{d2}$ and $P^+_{740}Pheo^-_{a3}$ radical pairs is in accordance with the analysis of electron-nuclear hyperfine couplings on the stably photo-accumulated A_0^- radical monitored by continuous wave and pulsed EPR spectroscopy in the Chl-*a* containing PSI [32,33]. Through this approach a 3:1 electron spin density delocalisation between the Chl *a* molecules at the eC2 and eC3 sites was estimated, implying rapid electron exchange between these cofactors. Despite substantially different chemical nature of the cofactors, the delocalisation of the unpaired electron within the eC2:eC3 Chl-*a* dimer is very close to the one estimated here for the Chl-*d*:Pheo-*a* heterodimer, at the equivalent position in the PSI from *A. marina*. Hence, in *A. marina* PSI, A_0 might therefore also be considered as an electronically coupled cofactor dimer. The direct population of $P^+_{700}A_0^-$ is supported by ultrafast TA measurements in the PSI from *Synechocystis* sp. PCC 6803, where the electronic properties of Chl-*a* at the $eC2_A$ and $eC2_B$ sites were altered by mutagenesis of the cofactor binding niches [31,60,61]. The kinetics in the wild type and PSI mutants were interpreted in terms of extremely rapid redistribution of the unpaired electron amongst the identified intermolecular radical pair states [62], occurring before the donation to the successive acceptors A_{1A} or A_{1B}.

On the other hand, a different reaction scheme for primary charge separation and charge stabilisation reactions in the Chl-*a* containing PSI, which does not imply the existence of a fast equilibrium between the radical states RP_1 and RP_2, has also been suggested in several studies [34–36,63,64]:

$$\mathrm{Ant}\Big/\mathrm{RC}^* \underset{k_{1-}}{\overset{k_1}{\rightleftarrows}} \mathrm{RP}_1 \overset{k_2}{\rightarrow} \mathrm{RP}_2 \qquad \text{(Scheme 1)}$$

According to these results, the primary radical pair RP_1 is in equilibrium with the antenna and reaction centre excited states (Ant/RC*), while charge stabilisation is ascribed to the further, substantially irreversible, electron transfer step.

The charge stabilisation mechanism in Scheme 1 differs from that suggested for the Chl-*d* containing PSI from *A. marina* in this paper (see Section 3.2). Yet, regardless of the exact scenario of the primary events in the Chl-*a* containing PSI, the stabilised radical pair $P^+_{700}Chl^-_{a3}$ is analogous to the $P^+_{740}Pheo^-_{a3}$ pair in *A. marina*, which allows to directly compare the redox-properties of Chl_{a3} and $Pheo_{a3}$.

4.2. Energetics of the ultrafast reactions in the photosystem I of A. marina

The energy gap ΔG_{RP_2} for the $P^+_{740}Pheo^-_{a3}$ radical pair formation is related to the equilibrium midpoint redox potential of $Pheo_{a3}$ by the energy balance [46,65,66]:

$$h\nu_0 = q_e E_m\left(P^+_{740}/P_{740}\right) - q_e E_m\left(Pheo_{a3}/Pheo^-_{a3}\right) + \Delta\varphi_{P^+_{740}Pheo^-_{a3}} - \Delta G_{RP_2} \qquad (1)$$

where $h\nu_0$ is the excitation energy of RC*, q_e is the elementary charge, $\Delta\varphi_{P^+_{740}Pheo^-_{a3}}$ is the electrostatic interaction of P^+_{740} and $Pheo^-_{a3}$. Considering that $\nu_0 \approx 740$ nm, the equilibrium midpoint potential $E_m = +450$ mV for P^+_{740}/P_{740} [18–20], and that the energy gap between RC* and $P^+_{740}Pheo^-_{a3}$ is ~60 meV, the operating redox potential of the $Pheo^-_{a3}$ anion could be estimated as −1.17 V. Differently from the equilibrium E_m, which could be obtained by redox-titration, the operating redox potential takes into account the $\Delta\varphi_{P_{740}Pheo_3}$ contribution. This difference is important for correct comparison of the redox-potentials of the cofactors in different proteins by various approaches. Further in the discussion of PSI energetics only the operating redox potentials will be considered.

The E_m value of the cofactor occupying the eC3 position in the PSI of *A. marina* retrieved from the kinetic analysis shall be compared with the one of the corresponding Chl-*a* cofactor in the canonical PSI, derived from comparable experimental approaches. Taking the oxidation midpoint potential of P_{700}/P^+_{700} pair equal to +450 mV [20,67,68], the excitation energy of 1.77 V and the energy gap between RC* and the $P^+_{700}A_0^-$ radical pair between 30 and 250 meV [35,36,46,64,69–72], the redox potential of Chl-*a* in eC3 position falls in a relatively large range of -(1.07–1.25) V. The uncertainty in the estimation of A_0^- potential is associated to the different mechanism of charge stabilisation discussed above. When considering reaction mechanisms represented by Scheme 1, the anion of Chl-*a* at the eC3 site has almost the same potential as $Pheo^-_{a3}$. On the other hand, when considering reaction mechanism analogous to the one obtained here for the PSI of *A. marina*, the operational potential of A_0^- is about 100 mV more negative than that of $Pheo^-_{a3}$. This difference is comparable to the one determined in between the E_m values of Chl-*a* and Pheo-*a* in organic solvents [73,74], i.e. ~200 mV. Within these energetic configurations, the substitution of Chl-*a* with Pheo-*a* at the eC3 site of *A. marina* PSI provides then an almost perfect compensation for the energy loss in between P_{740}* and P_{700}*. A comparison of the energy levels, according to the latter scenario, for Chl-*a*-binding PSI and PSI form *A. marina* is shown in Fig. 8 A,B. It is also worth noting that the reduction potential of Chl-*d* in aprotic solvents is by 180 mV more positive than E_m of Chl-*a* [73], as well. Hence, from this point of view, Chl-*d* at the eC3 site could act analogously to Pheo-*a*, which is instead present in the *A. marina* photosystem.

As discussed in the successive paragraph, the presence of Pheo-*a* at the eC3 might be required because of structural rather than energetic constraints.

On the other hand, when considering the energetics related to the next stage of charge stabilisation, the Chl-*a* to Pheo-*a* substitution should slow down the $A_0 \rightarrow A_1$ transition in *A. marina* compared to the canonical PSI. However, the rate of $A_0 \rightarrow A_1$ transition depends very little on the driving force: a decrease in the energy gap by 300 meV in the PSI complexes with 2-amino-AQ substituted for phylloquinone slowed down the lifetime of A_1 reduction from 23 ps to only 35 ps [75,76], which is in line with a minor slowdown of this reaction in *A. marina* (28 ps) compared to the canonical PSI.

4.3. Structural interactions of chlorin macrocycles at the eC2 and eC3 sites of photosystem I

The comparison of the PSI structures from *A. marina* [22,26], and *T. elongatus* [2] revealed two remarkable distinctions in the protein surrounding of the eC2 and eC3 cofactors.

The first one is the replacement of the small side chain of $Leu531_{PsaA}$ by the bulky one of Phe (numbered as Phe528) in the PsaA of *A. marina* (Fig. 9). As a result, whereas in the PSI from *T. elongatus* the vinyl group of Chl-*a* in the $eC2_A$ site is turned in the opposite direction from the chlorin ring of Chl-*a* in the $eC3_A$ site, in *A. marina* the respective aldehyde group of Chl-*d* in the $eC2_A$ site is turned towards the Pheo-*a* in the $eC3_A$ site. Hence, the polar carbonyl oxygen of Chl_{d2} does not lie in the plane of macrocycle, but interacts directly with the macrocycle of $Pheo_{a3}$ (Fig. 9B).

Such a direct interaction of Chl_{d2} and $Pheo_{a3}$ via the carbonyl oxygen of Chl_{d2} (distance of 3.2 Å) should result in a high electronic coupling of both macrocycles that is consistent with the fast electron exchange between Chl_{d2} and $Pheo_{a3}$. Moreover, it leads to a significant out-of-plane distortion of the Chl_{d2} and $Pheo_{a3}$ macrocycles, which should decrease their reduction potentials relative to the midpoint potentials of their flat conformations in solution. The effects of out-of-plane macrocycle displacements on the reorganization energy of non-planar chlorin reduction have a magnitude of 0.5–0.8 eV [77]. Both effects together may explain the simultaneous kinetic evolution of the Chl_{d2} and $Pheo_{a3}$ observed in this study (see Table 2 and Fig. 7A).

It is worth noting that the estimated potential of $Pheo^-_{a3}$ in the PSI from *A. marina* is by ~0.4 V more negative than in the protein environment of PSII, where its E_m value was determined in the range of –(0.5–0.6) V [57,78–80] (Fig. 8C). These values were obtained in equilibrium conditions by redox titration, thus they do not include the positive effect of the P_{680} cation. This nonetheless highlights a strong influence of the protein environment on the redox potentials of the

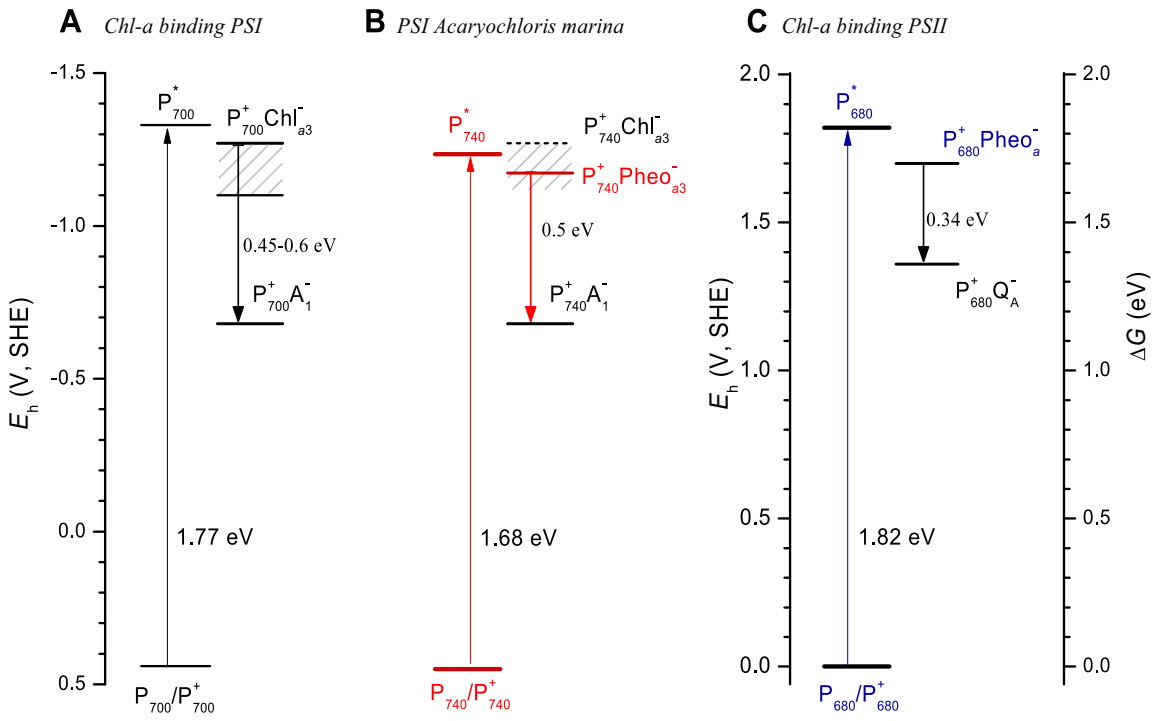

Fig. 8. Energetics of primary charge separation and successive ET steps in different photosystems: canonical Chl-*a* binding PSI (A), Chl-*d* binding PSI of *A. marina* (B) and Chl-*a* binding PSII (C). The energetic parameters for Chl-*a* PSI represent indicative mean values from the literature, except for the A_0 potential for which a range of values, indicated by the shaded areas, is presented (see main text for further details). The energetics parameters for *A. marina* PSI were derived from the kinetic modelling of TA data in this study.

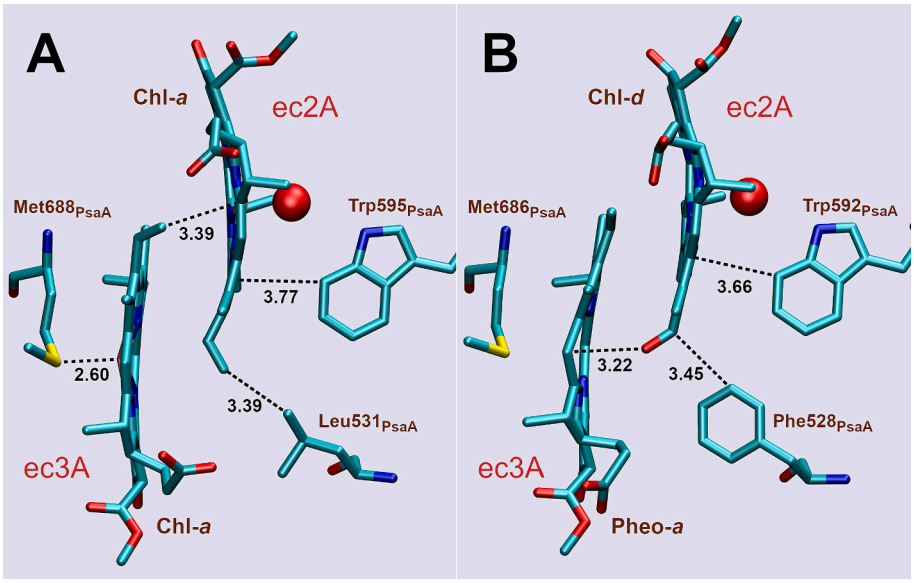

Fig. 9. Interactions of chlorin macrocycles in the $eC2_A$ and $eC3_A$ sites with nearby amino acid residues in the A-branch of redox cofactors in PSI complexes from *T. elongatus* [2] (A) and *A. marina* [22] (B). The closest van der Waals contacts are indicated by dashed lines. The water molecules coordinating the Mg atoms in the $eC2_A$ sites are shown by red spheres. (For interpretation of the references to colour in this figure legend, the reader is referred to the web version of this article.)

electron transfer cofactors, that are however not exceptional [70]. From the structural point of view, the negative shift of the Pheo-*a* midpoint potential in *A. marina* PSI might be partially explained by the fact that the chlorin ring of $Pheo_{a3}$ is bent out of plane, whereas the chlorin ring of the Pheo-*a* molecule in the PSII complex is perfectly flat [81].

Another remarkable point is that the Mg atom of Chl-*a* at eC2 site in the PSI from *T. elongatus*, being coordinated by a water molecule from one side of the chlorin plane (red sphere in Fig. 9A), is in a direct contact with the non-polar vinyl group of Chl-*a* at eC3 from the other side. If the eC3 binding site in the PSI from *A. marina* would be occupied by Chl-*d*, the presence of the polar aldehyde group will result in a conformational change, where the Chl-*d* at eC2 would likely be six-coordinated (by water and by carbonyl oxygen), which is an exergonic configuration for a protein environment [82]. This might be a further argument to rationalise the presence of Pheo-*a* in the eC3 position, and the tuning of its potential towards more reducing values.

The second distinctive feature, surprisingly concerns only the PsaB subunit where the methionine residue Met668$_{PsaB}$ acting as the axial ligand to Chl-*a* in the eC3$_B$ site of canonical PSI is replaced, in *A. marina*, by a leucine [83], which is incapable of direct Chl coordination. Site directed mutants targeting the A$_0$/eC3 axial ligation have been quite intensively investigated in Chl-*a*-binding PSI. There is a general consensus that substitutions of the PsaA residue Met688, acting as ligand to A$_{0A}$, in PSI result in slower trapping [64,84–89]. A significant slowing of electron transfer kinetics was observed also in the PSI variants, where the equivalent residue Met668 affecting A$_{0B}$ coordination, was substituted in the symmetrical B-branch [84,85,87,89]. Moreover, modifications of the eC2/eC3 sites affected the relative utilisation of the two active branches [31,64,71,84–94]. The presence of a leucine in place of a methionine in the Pheo-*a* binding niche of the PsaB subunit of *A. marina*, shall however be less relevant than in the case of canonical PSI, since Pheo-*a* lacks the central Mg and hence direct axial coordination cannot occur.

However, interestingly, the weakening of the coordination induced by Met-to-Leu and Met-to-Asn substitutions of Met688$_{PsaA}$ in *Synechocystis* sp. PCC 6803 caused an heterogeneity in the phylloquinone A$_1$ reduction slowing it from 24 ps to 30–100 ps [86], an effect that resembles the heterogeneous Pheo-*a* oxidation kinetics observed in *A. marina* (compare Fig. 5 and Fig. 5 in [86]). The polyphasic kinetics observed in the Met-to-Asn *Synechocystis* mutants was explained in terms of an increased flexibility of Asn coordination to eC3$_A$ [88]. By analogy, it can be hypothesised, that the absence of direct coordination to Pheo-*a* of *A. marina* PSI, increase the degree of conformational freedom within the cofactor coordination niches in both RC subunits, resulting in the observed heterogeneous kinetics.

4.4. Effects of pheophytin a on the energy transfer dynamics in photosystem I

The substitution of Chl-*a* by Pheo-*a* in the eC3$_A$/eC3$_B$ positions, being possibly necessary for the charge stabilisation within the RC, might, on the other hand, negatively affect the efficiency of excited state energy delivery from the antenna to the RC because of the large difference in its electronic transition with respect to the majority of the antenna chromophores.

The energy transfer between spatially separated pigments is determined by two factors: the dipole-dipole interaction of their transition moments, and the spectral overlap of the excitation donor and acceptor (it includes nuclear overlap factors, separated from the electronic coupling in the form of Franck-Condon factors) [95] The transfer of excitation energy from the antenna to the RC was analysed using various approximations to account for the pairwise dipole-dipole interactions and the electron-phonon coupling of all pigments composing the antenna and the RC [96–99]. In all approximations, the main channels for energy transfer to the RC are the excitonically coupled pairs A40-eC3$_A$ and B36-eC3$_A$ in the outer part of antenna, and the B39-eC3$_B$ pair in the central part of antenna [96–99]. The dual Chl$_{a2}$ → Chl$_{d2}$ and Chl$_{a3}$ → Pheo$_{a3}$ substitutions, only slightly affect the dipole-dipole interactions, but significantly decrease the excitonic interaction of pigments in the RC. Unlike the canonical PSI, the spectra of Pheo-*a* and Chl-*d* do only weakly overlap (Fig. S13) since the energy of the excitation acceptor (Pheo-*a* in the eC3 site) significantly exceeds the energy of the excitation donor (Chl-*d* in the antenna). For this reason, the main energy acceptor in the reaction centre of PSI from *A. marina* should not be Pheo-*a* but Chl-*d* in the eC2 position, which has an absorption maximum at 715 nm (Fig. 7E). Therefore, some decrease in the efficiency of excitation energy transfer from antenna to RC may be expected.

The observed time of energy trapping within RC depends on the presence of low-energy Chl forms in the antenna: the fewer is the fraction of LWC, the faster is the kinetics of energy transfer to the RC and the subsequent formation of radical pair states (e.g. [36,100–102]). Under conditions of far-red excitation at room temperature in the canonical PSI from *Synechocystis* sp. PCC 6803, which contains a minimal fraction of LWC [103,104], the energy transfer from the antenna to the RC occurs on a time scale of 2–4 ps [62,99,101]. In the PSI from *A. marina*, the energy level of the special pair P$_{740}$ is at the far-red edge of the absorption spectrum (see [22] and Fig. S6). The main components of P$_{740}$ oxidation, monitored by the absorption band at 470 nm, are found in the time range of 10 and 20 ps for the selective (740 nm) and unselective (630 nm) excitation, respectively (Fig. 6D and E). The observed slowing of the energy trapping compared to the canonical PSI from *Synechocystis* sp. PCC 6803 may be due to the exclusion of the eC3$_A$/eC3$_B$ sites from the possible pathways of energy transfer to the RC.

Kinetic modelling gives an estimate of the rate constant $k_{12} = 560$ ns^{-1} (lifetime of 1.8 ps) for the primary reaction of charge separation in the RC (see the kinetic scheme in Fig. 7A). The compartment [RC*] employed in kinetic modelling of the data might be subject to some ambiguity and have therefore different structural and functional interpretations. In this context, attribution of the transient spectrum of exited RC (Fig. 7D) to certain pigments of the molecular structure is of considerable interest.

In the most straightforward assignment, the compartment [RC*] represents an ensemble of four Chl-*d* molecules comprising the reaction centre itself, i.e. two molecules of the special pair P$_{740}$ and two Chl-*d* monomers bound in the eC2$_A$ and eC2$_B$ sites, and eventually the weakly excitonically coupled Pheo-*a* molecules. Yet it cannot be completely excluded, that the [RC*] compartment may also include contributions from an ensemble of excitonically coupled Chl-*d* molecules in the antenna, which very rapidly donate and equilibrate with the RC proper, becoming then kinetically indistinguishable from it. The transient spectrum of the [RC], presented in Fig. 7D, includes two bleaching bands of similar amplitude with minima at 718 and 730 nm. The difference spectrum of the primary $P^+_{740}Chl^-_{d2}$ ion-radical state, shown in Fig. 7E, has a major minimum at 715 nm (attributed to the Chl$_{d2}$ monomers in the eC2$_A$/eC2$_B$ positions) and a broad minor bleaching at 740 nm (attributable to the P$_{740}$ cation, see the spectrum of $P^+_{740}A^-_1$ in Fig. 7F). Since the spectra of the excited [RC] and the primary $P^+_{740}Chl^-_{d2}$ ion-radical state are similar in the 710–720 nm window, but differ around 730 nm, a contribution of rapidly equilibrated antenna molecules to the kinetically retrieved [RC*] compartment cannot be excluded. In this case, the rate constant $k_{12} = 560$ ns^{-1} refers partially to processes of energy transfer from some pigments with the Q$_Y$ band located at 730 nm to the RC pigments. In recent calculations, Kimura et al. [105] identified a group of excitonically coupled pigments, the energy level of which is higher than the energy of the pigments of the RC and which can act as an excitation donor for the latter. In this group of pigments, the Chl monomer #A1132 (numbered according to the canonical structure 1JB0 [2]) is closest to the eC2$_B$ position. Direct excitation of this group of pigments by the 740 nm pulse can explain the fast charge separation observed in a small fraction of the complexes (Fig. 6E).

5. Conclusions

1. Due to the unique cofactor composition of the *A. marina* PSI it became possible to clearly distinguish the primary charge separation and successive electron transfer steps in the isolated PSI complexes.
2. The primary and secondary ion-radical pairs were identified as $P^+_{740}Chl^-_{d2}$ and $P^+_{740}Pheo^-_{a3}$, respectively.
3. The collected data allowed to exclude the involvement of Chl-*a* in either photochemical or electron transfer reactions in PSI of *A. marina*.
4. The rate of the electron transfer reaction from $P^+_{740}Chl^-_{d2}$ to $P^+_{740}Pheo^-_{a3}$ was estimated to be faster than 1 ps, and because of a low equilibrium constant, the electron density is rapidly shared between the $P^+_{740}Chl^-_{d2}$ and the $P^+_{740}Pheo^-_{a3}$radical pairs.

5. The value of the operating redox potential of $Pheo_{a3}^{-}$ in *A. marina* PSI was estimated as −1.17 V, which is 0.6–0.7 V more negative than the E_m value of Pheo-*a* in Chl-*a* binding PSII.
6. The comparative analysis of the structures of PSI from *A. marina* and *T. elongatus* revealed the structural restriction on the Chl-*d* presence in the eC3 binding site.

Declaration of competing interest

The authors have no conflicts of interest to declare.

Data availability

Data will be made available on request.

Acknowledgments

This work was supported by the Russian Science Foundation Grant RSF 21-74-10085.

SS and APC acknowledge support from Fondazione Cariplo (CYAO project, grant number 2016-0667) and from Regione Lombardia through the project "Enhancing Photosynthesis" (DSS 16652 30/11/2021) on behalf of the winners of the "Lombardia è Ricerca – 2020" award.

Appendix A. Supplementary data

Supplementary data to this article can be found online at https://doi.org/10.1016/j.bbabio.2023.148984.

References

[1] J.H.A. Nugent, S. Purton, M.C.W. Evans, Oxygenic Photosynthesis in Algae and Cyanobacteria: Electron Transfer in Photosystems I and II, Springer, Dordrecht, 2003, pp. 133–156.
[2] P. Jordan, P. Fromme, H.T. Witt, O. Klukas, W. Saenger, N. Krauß, Three-dimensional structure of cyanobaoterial photosystem I at 25 Å resolution, Nature 411 (2001) 909–917.
[3] H. Miyashita, H. Ikemoto, N. Kurano, K. Adachi, M. Chihara, S. Miyachi, Chlorophyll d as a major pigment, Nature 383 (1996) 402.
[4] H. Miyashita, K. Adachi, N. Kurano, H. Ikemoto, M. Chihara, S. Miyachi, Pigment composition of a novel oxygenic photosynthetic prokaryote containing chlorophyll d as the major chlorophyll, Plant Cell Physiol. 38 (1997) 274–281.
[5] M. Kühl, M. Chen, P.J. Ralph, U. Schreiber, A.W.D. Larkum, Ecology: a niche for cyanobacteria containing chlorophyll d, Nature 433 (2005) 820.
[6] F. Gan, S. Zhang, N.C. Rockwell, S.S. Martin, J.C. Lagarias, D.A. Bryant, Extensive remodeling of a cyanobacterial photosynthetic apparatus in far-red light, Science 345 (2014) 1312–1317.
[7] M. Chen, Y. Li, D. Birch, R.D. Willows, A cyanobacterium that contains chlorophyll f - a red-absorbing photopigment, FEBS Lett. 586 (2012) 3249–3254.
[8] D.J. Nürnberg, J. Morton, S. Santabarbara, A. Telfer, P. Joliot, L.A. Antonaru, A. V. Ruban, T. Cardona, E. Krausz, A. Boussac, A. Fantuzzi, A. William Rutherford, Photochemistry beyond the red limit in chlorophyll f–containing photosystems, Science 360 (2018) 1210–1213.
[9] D.A. Cherepanov, I.V. Shelaev, F.E. Gostev, A.V. Aybush, M.D. Mamedov, G. Shen, V.A. Nadtochenko, D.A. Bryant, A.Y. Semenov, J.H. Golbeck, Evidence that chlorophyll f functions solely as an antenna pigment in far-red-light photosystem I from Fischerella thermalis PCC 7521, Biochim. Biophys. Acta Bioenerg. 1861 (2020).
[10] H. Schiller, H. Senger, H. Miyashita, S. Miyachi, H. Dau, Light-harvesting in Acaryochloris marina - spectroscopic characterization of a chlorophyll d-dominated photosynthetic antenna system, FEBS Lett. 410 (1997) 433–436.
[11] M. Kobayashi, S. Akutsu, D. Fujinuma, H. Furukawa, H. Komatsu, Y. Hotota, Y. Kato, Y. Kuroiwa, T. Watanabe, M. Ohnishi-Kameyama, H. Ono, S. Ohkubo, H. Miyashit, Physicochemical Properties of Chlorophylls in Oxygenic Photosynthesis — Succession of co-Factors from Anoxygenic to Oxygenic Photosynthesis, in: Z. Dubinsky (Ed.), Photosynthesis, 2013, pp. 47–90.
[12] D.M. Niedzwiedzki, R.E. Blankenship, Singlet and triplet excited state properties of natural chlorophylls and bacteriochlorophylls, Photosynth. Res. 106 (2010) 227–238.
[13] D.A. Cherepanov, A.A. Petrova, M.D. Mamedov, A.I. Vishnevskaya, F.E. Gostev, I. V. Shelaev, A.V. Aybush, V.A. Nadtochenko, Comparative absorption dynamics of the singlet excited states of chlorophylls a and d, Biochem. Mosc. 87 (2022) 1179–1186.
[14] T. Tomo, S.I. Allakhverdiev, M. Mimuro, Constitution and energetics of photosystem i and photosystem II in the chlorophyll d-dominated cyanobacterium Acaryochloris marina, J. Photochem. Photobiol. B Biol. 104 (2011) 333–340.
[15] Q. Hu, H. Miyashita, I. Iwasaki, N. Kurano, S. Miyachi, M. Iwaki, S. Itoh, A photosystem I reaction center driven by chlorophyll d in oxygenic photosynthesis, Proc. Natl. Acad. Sci. U. S. A. 95 (1998) 13319–13323.
[16] H. Mino, A. Kawamori, D. Aoyama, T. Tomo, M. Iwaki, S. Itoh, Proton ENDOR study of the primary donor P740+, a special pair of chlorophyll d in photosystem i reaction center of Acaryochloris marina, Chem. Phys. Lett. 411 (2005) 262–266.
[17] V. Sivakumar, R. Wang, G. Hastings, Photo-oxidation of P740, the primary Electron donor in photosystem I from Acaryochloris marina, Biophys. J. 85 (2003) 3162–3172.
[18] T. Tomo, Y. Kato, T. Suzuki, S. Akimoto, T. Okubo, T. Noguchi, K. Hasegawa, T. Tsuchiya, K. Tanaka, M. Fukuya, N. Dohmae, T. Watanabe, M. Mimuro, Characterization of highly purified photosystem I complexes from the chlorophyll d-dominated cyanobacterium Acaryochloris marina MBIC 11017, J. Biol. Chem. 283 (2008) 18198–18209.
[19] B. Bailleul, X. Johnson, G. Finazzi, J. Barber, F. Rappaport, A. Telfer, The thermodynamics and kinetics of electron transfer between cytochrome b6f and photosystem I in the chlorophyll d-dominated cyanobacterium, Acaryochloris marina, J. Biol. Chem. 283 (2008) 25218–25226.
[20] M. Schenderlein, M. Çetin, J. Barber, A. Telfer, E. Schlodder, Spectroscopic studies of the chlorophyll d containing photosystem I from the cyanobacterium, Acaryochloris marina, Biochim. Biophys. Acta Bioenerg. 1777 (2008) 1400–1408.
[21] H. Witt, E. Bordignon, D. Carbonera, J.P. Dekker, N. Karapetyan, C. Teutloff, A. Webber, W. Lubitz, E. Schlodder, Species-specific differences of the spectroscopic properties of P700: analysis of the influence of non-conserved amino acid residues by site-directed mutagenesis of photosystem I from Chlamydomonas reinhardtii, J. Biol. Chem. 278 (2003) 46760–46771.
[22] T. Hamaguchi, K. Kawakami, K. Shinzawa-Itoh, N. Inoue-Kashino, S. Itoh, K. Ifuku, E. Yamashita, K. Maeda, K. Yonekura, Y. Kashino, Structure of the far-red light utilizing photosystem I of Acaryochloris marina, Nat. Commun. 12 (2021) 1–10.
[23] S. Ohashi, H. Miyashita, N. Okada, T. Iemura, T. Watanabe, M. Kobayashi, Unique photosystems in Acaryochloris marina, Photosynth. Res. 98 (2008) 141–149.
[24] S. Itoh, H. Mino, K. Itoh, T. Shigenaga, T. Uzumaki, M. Iwaki, Function of chlorophyll d in reaction centers of photosystems I and II of the oxygenic photosynthesis of Acaryochloris marina, Biochemistry 46 (2007) 12473–12481.
[25] S. Kumazaki, K. Abiko, I. Ikegami, M. Iwaki, S. Itoh, Energy equilibration and primary charge separation in chlorophyll d-based photosystem I reaction center isolated from Acaryochloris marina, FEBS Lett. 530 (2002) 153–157.
[26] C. Xu, Q. Zhu, J. Chen, L. Shen, X. Yi, Z. Huang, W. Wang, M. Chen, T. Kuang, J. Shen, X. Zhang, G. Han, A unique photosystem I reaction center from a chlorophyll d -containing cyanobacterium Acaryochloris marina, J. Integr. Plant Biol. 63 (2021) 1740–1752.
[27] R.A. Khatypov, A.Y. Khmelnitskiy, M.M. Leonova, L.G. Vasilieva, V.A. Shuvalov, Primary light-energy conversion in tetrameric chlorophyll structure of photosystem II and bacterial reaction centers: I a review, Photosynth. Res. 98 (2008) 81–93.
[28] S. Savikhin, R. Jankowiak, Mechanism of primary charge separation in photosynthetic reaction centers, in: J. Golbeck, A. van der Est (Eds.), Biophys. Photosynth., Springer New York, New York, NY, 2014, pp. 193–240.
[29] D.A. Cherepanov, I.V. Shelaev, F.E. Gostev, M.D. Mamedov, A.A. Petrova, A. V. Aybush, V.A. Shuvalov, A.Y. Semenov, V.A. Nadtochenko, Mechanism of adiabatic primary electron transfer in photosystem I: femtosecond spectroscopy upon excitation of reaction center in the far-red edge of the Q Y band, Biochim. Biophys. Acta Bioenerg. 2017 (1858) 895–905.
[30] I.V. Shelaev, F.E. Gostev, M.D. Mamedov, O.M. Sarkisov, V.A. Nadtochenko, V. A. Shuvalov, A.Y. Semenov, Femtosecond primary charge separation in Synechocystis sp PCC 6803 photosystem I, Biochim. Biophys. Acta Bioenerg. 1797 (2010) 1410–1420.
[31] D.A. Cherepanov, I.V. Shelaev, F.E. Gostev, V.A. Nadtochenko, W. Xu, J. H. Golbeck, A.Y. Semenov, Symmetry breaking in photosystem I: ultrafast optical studies of variants near the accessory chlorophylls in the A- and B-branches of electron transfer cofactors, Photochem. Photobiol. Sci. 20 (2021) 1209–1227.
[32] M. Gorka, A. Baldansuren, A. Malnati, E. Gruszecki, J.H. Golbeck, K.V. Lakshmi, Shedding light on primary donors in photosynthetic reaction centers, Front. Microbiol. 12 (2021) 2776.
[33] M. Gorka, P. Charles, V. Kalendra, A. Baldansuren, K.V. Lakshmi, J.H. Golbeck, A dimeric chlorophyll electron acceptor differentiates type I from type II photosynthetic reaction centers, IScience 24 (2021), 102719.
[34] M.G. Müller, J. Niklas, W. Lubitz, A.R. Holzwarth, Ultrafast transient absorption studies on photosystem I reaction centers from Chlamydomonas reinhardtii 1 a new interpretation of the energy trapping and early Electron transfer steps in photosystem I, Biophys. J. 85 (2003) 3899–3922.
[35] M.G. Müller, C. Slavov, R. Luthra, K.E. Redding, A.R. Holzwarth, Independent initiation of primary electron transfer in the two branches of the photosystem I reaction center, Proc. Natl. Acad. Sci. U. S. A. 107 (2010) 4123–4128.
[36] E. Molotokaite, W. Remelli, A.P. Casazza, G. Zucchelli, D. Polli, G. Cerullo, S. Santabarbara, Trapping dynamics in photosystem I-light harvesting complex I of higher plants is governed by the competition between excited state diffusion from low energy states and photochemical charge separation, J. Phys. Chem. B 121 (2017) 9816–9830.
[37] D. Mi, M. Chen, S. Lin, M. Lince, A.W.D. Larkum, R.E. Blankenship, Excitation dynamics in the core antenna in the photosystem I reaction center of the chlorophyll d-containing photosynthetic prokaryote acaryochloris marina, J. Phys. Chem. B 107 (2003) 1452–1457.

[38] B. Gobets, R. Van Grondelle, Energy transfer and trapping in photosystem I, Biochim. Biophys. Acta Bioenerg. 1507 (2001) 80–99.
[39] B. Gobets, I.H. van Stokkum, M. Rögner, J. Kruip, E. Schlodder, N.V. Karapetyan, J.P. Dekker, R. van Grondelle, Time-resolved fluorescence emission measurements of photosystem I particles of various cyanobacteria: a unified compartmental model, Biophys. J. 81 (2001) 407–424.
[40] N.V. Karapetyan, D. Dorra, G. Schweitzer, I.N. Bezsmertnaya, A.R. Holzwarth, Fluorescence spectroscopy of the longwave chlorophylls in trimeric and monomeric photosystem I core complexes from the cyanobacterium Spirulina platensis, Biochemistry 36 (1997) 13830–13837.
[41] S. Turconi, J. Kruip, G. Schweitzer, M. Rögner, A.R. Holzwarth, A comparative fluorescence kinetics study of photosystem I monomers and trimers from Synechocystis PCC 6803, Photosynth. Res. 49 (1996) 263–268.
[42] S. Savikhin, W. Xu, P.R. Chitnis, W.S. Struve, Ultrafast primary processes in PS I from Synechocystis sp PCC 6803: roles of P700 and A0, Biophys. J. 79 (2000) 1573–1586.
[43] A.N. Melkozernov, S. Lin, R.E. Blankenship, Femtosecond transient spectroscopy and Excitonic interactions in photosystem I, J. Phys. Chem. B 104 (2000) 1651–1656.
[44] A. Chauvet, N. Dashdorj, J.H. Golbeck, T.W. Johnson, S. Savikhin, Spectral resolution of the primary electron acceptor A0 in photosystem I, J. Phys. Chem. B 116 (2012) 3380–3386.
[45] D.A. Cherepanov, N.G. Brady, I.V. Shelaev, J. Nguyen, F.E. Gostev, M. D. Mamedov, V.A. Nadtochenko, B.D. Bruce, PSI-SMALP, a detergent-free cyanobacterial photosystem I, reveals faster femtosecond photochemistry, Biophys. J. 118 (2020) 337–351.
[46] K. Brettel, Electron transfer and arrangement of the redox cofactors in photosystem I, Biochim. Biophys. Acta Bioenerg. 1318 (1997) 322–373.
[47] S. Santabarbara, B. Bailleul, K. Redding, J. Barber, F. Rappaport, A. Telfer, Kinetics of phyllosemiquinone oxidation in the photosystem i reaction Centre of Acaryochloris marina, Biochim. Biophys. Acta Bioenerg. 2012 (1817) 328–335.
[48] S. Santabarbara, M. Chen, A.W.D. Larkum, M.C.W. Evans, An electron paramagnetic resonance investigation of the electron transfer reactions in the chlorophyll d containing photosystem I of Acaryochloris marina, FEBS Lett. 581 (2007) 1567–1571.
[49] T.W. Johnson, B. Zybailov, A.D. Jones, R. Bittl, S. Zech, D. Stehlik, J.H. Golbeck, P.R. Chitnis, Recruitment of a foreign quinone into the A1 site of photosystem I: in vivo replacement of plastoquinone-9 by media-supplemented naphthoquinones in phylloquinone biosynthetic pathway mutants of synechocystis sp PCC 6803, J. Biol. Chem. 276 (2001) 39512–39521.
[50] A.L. Dobryakov, J.L. Pérez Lustres, S.A. Kovalenko, N.P. Ernsting, Femtosecond transient absorption with chirped pump and supercontinuum probe: perturbative calculation of transient spectra with general lineshape functions, and simplifications, Chem. Phys. 347 (2008) 127–138.
[51] E.N. Golubeva, E.M. Zubanova, M.Y. Melnikov, F.E. Gostev, I.V. Shelaev, V. A. Nadtochenko, Femtosecond spectroscopy and TD-DFT calculations of CuCl 4 2− excited states, Dalt. Trans. 43 (2014) 17820–17827.
[52] S.W. Provencher, CONTIN: a general purpose constrained regularization program for inverting noisy linear algebraic and integral equations, Comput. Phys. Commun. 27 (1982) 229–242.
[53] V.H. Segtnan, Š. Šašić, T. Isaksson, Y. Ozaki, Studies on the structure of water using two-dimensional near-infrared correlation spectroscopy and principal component analysis, Anal. Chem. 73 (2001) 3153–3161.
[54] D.Y. Tzeng, R.S. Berns, A review of principal component analysis and its applications to color technology, Color. Res. Appl. 30 (2005) 84–98.
[55] D.A. Cherepanov, F.E. Gostev, I.V. Shelaev, A.V. Aibush, M.D. Mamedov, V. A. Shuvalov, A.Y. Semenov, V.A. Nadtochenko, Visible and near infrared absorption Spectrum of the excited singlet state of chlorophyll a, High Energy Chem. 54 (2020) 145–147.
[56] I. Fujita, M.S. Davis, J. Fajer, Anion radicals of pheophytin and chlorophyll a: their role in the primary charge separations of plant photosynthesis, J. Am. Chem. Soc. 100 (1978) 6280–6282.
[57] V.V. Klimov, S.I. Allekhverdiev, S. Demeter, A.A. Krasnovsky, Photoreduction of pheophytin in photosystem II of chloroplasts as a function of redox potential of the medium, Dokl. Akad. Nauk USSR 249 (1979) 227–230.
[58] A.A. Zabelin, V.A. Shkuropatova, Z.K. Makhneva, A.A. Moskalenko, V. A. Shuvalov, A.Y. Shkuropatov, Chemically modified reaction centers of photosystem II: exchange of pheophytin a with 7-deformyl-7-hydroxymethyl-pheophytin b, Biochim. Biophys. Acta Bioenerg. 2014 (1837) 1870–1881.
[59] C. Eijckelhoff, J.P. Dekker, A routine method to determine the chlorophyll a, pheophytin a and β-carotene contents of isolated photosystem II reaction center complexes, Photosynth. Res. 52 (1997) 69–73.
[60] S.L. Badshah, J. Sun, S. Mula, M. Gorka, P. Baker, R. Luthra, S. Lin, A. van der Est, J.H. Golbeck, K.E. Redding, Mutations in algal and cyanobacterial photosystem I that independently affect the yield of initial charge separation in the two electron transfer cofactor branches, Biochim. Biophys. Acta Bioenerg. 2018 (1859) 42–55.
[61] D.A. Cherepanov, I.V. Shelaev, F.E. Gostev, A. Petrova, A.V. Aybush, V. A. Nadtochenko, W. Xu, J.H. Golbeck, A.Y. Semenov, Primary charge separation within the structurally symmetric tetrameric Chl2APAPBChl2B chlorophyll exciplex in photosystem I, J. Photochem. Photobiol. B Biol. 217 (2021), 112154.
[62] D.A. Cherepanov, I.V. Shelaev, F.E. Gostev, A.V. Aybush, M.D. Mamedov, V. A. Shuvalov, A.Y. Semenov, V.A. Nadtochenko, Generation of ion-radical chlorophyll states in the light-harvesting antenna and the reaction center of cyanobacterial photosystem I, Photosynth. Res. 1–19 (2020).
[63] A.R. Holzwarth, M.G. Müller, J. Niklas, W. Lubitz, Charge recombination fluorescence in photosystem I reaction centers from Chlamydomonas reinhardtii, J. Phys. Chem. B 109 (2005) 5903–5911.
[64] W. Giera, V.M. Ramesh, A.N. Webber, I. van Stokkum, R. van Grondelle, K. Gibasiewicz, Effect of the P700 pre-oxidation and point mutations near A0 on the reversibility of the primary charge separation in photosystem I from Chlamydomonas reinhardtii, Biochim. Biophys. Acta Bioenerg. 1797 (2010) 106–112.
[65] N.W. Woodbury, W.W. Parson, Nanosecond fluorescence from chromatophores of Rhodopseudomonas sphaeroides and Rhodospirillum rubrum, BBA - Bioenerg. 850 (1986) 197–210.
[66] D.A. Cherepanov, A.Y. Semenov, M.D. Mamedov, A.V. Aybush, F.E. Gostev, I. V. Shelaev, V.A. Shuvalov, V.A. Nadtochenko, Current state of the primary charge separation mechanism in photosystem I of cyanobacteria, Biophys. Rev. 14 (2022) 805–820.
[67] A.N. Webber, H. Su, S.E. Bingham, H. Käss, L. Krabben, M. Kuhn, R. Jordan, E. Schlodder, W. Lubitz, Site-directed mutations affecting the spectroscopic characteristics and midpoint potential of the primary donor in photosystem I, Biochemistry 35 (1996) 12857–12863.
[68] A.N. Webber, W. Lubitz, P700: the primary electron donor of photosystem I, Biochim. Biophys. Acta Bioenerg. 1507 (2001) 61–79.
[69] V.A. Shuvalov, The study of the primary photoprocesses in photosystem I of chloroplasts recombination luminescence, chlorophyll triplet state and triplet-triplet annihilation, Biochim. Biophys. Acta Bioenerg. 430 (1976) 113–121.
[70] V.V. Ptushenko, D.A. Cherepanov, L.I. Krishtalik, A.Y. Semenov, Semi-continuum electrostatic calculations of redox potentials in photosystem I, Photosynth. Res. 97 (2008) 55–74.
[71] S. Santabarbara, P. Heathcote, M.C.W. Evans, Modelling of the electron transfer reactions in photosystem I by electron tunnelling theory: the phylloquinones bound to the PsaA and the PsaB reaction Centre subunits of PS I are almost isoenergetic to the iron-sulfur cluster FX, Biochim. Biophys. Acta Bioenerg. 1708 (2005) 283–310.
[72] F.A.M. Kleinherenbrink, G. Hastings, R.E. Blankenship, B.P. Wittmershaus, Delayed fluorescence from Fe-S type photosynthetic reaction centers at low redox potential, Biochemistry 33 (1994) 3096–3105.
[73] M. Kobayashi, S. Ohashi, K. Iwamoto, Y. Shiraiwa, Y. Kato, T. Watanabe, Redox potential of chlorophyll d in vitro, Biochim. Biophys. Acta Bioenerg. 1767 (2007) 596–602.
[74] M.R. Wasielewski, R.L. Smith, A.G. Kostka, Electrochemical production of chlorophyll a and pheophytin a excited states, J. Am. Chem. Soc. 102 (1981) 358.
[75] M. Iwaki, S. Kumazaki, K. Yoshihara, T. Erabi, S. Itoh, ΔG0 dependence of the electron transfer rate in the photosynthetic reaction center of plant photosystem I: natural optimization of reaction between chlorophyll a (A0) and quinone, J. Phys. Chem. 100 (1996) 10802–10809.
[76] D. Cherepanov, A. Aybush, T.W. Johnson, I. Shelaev, F. Gostev, M. Mamedov, V. Nadtochenko, A. Semenov, Inverted region in the reaction of the quinone reduction in the A1-site of photosystem I from cyanobacteria, Photosynth. Res. 1 (2023) 1–17, https://doi.org/10.1007/s11120-023-01020-2.
[77] T. Nakanishi, K. Ohkubo, T. Kojima, S. Fukuzumi, Reorganization energies of diprotonated and saddle-distorted porphyrins in photoinduced electron-transfer reduction controlled by conformational distortion, J. Am. Chem. Soc. 131 (2009) 577–584.
[78] Y. Kato, M. Sugiura, A. Oda, T. Watanabe, Spectroelectrochemical determination of the redox potential of pheophytin a, the primary electron acceptor in photosystem II, Proc. Natl. Acad. Sci. U. S. A. 106 (2009) 17365–17370.
[79] S.I. Allakhverdiev, T. Tomo, Y. Shimada, H. Kindo, R. Nagao, V.V. Klimov, M. Mimuro, Redox potential of pheophytin a in photosystem II of two cyanobacteria having the different special pair chlorophylls, Proc. Natl. Acad. Sci. U. S. A. 107 (2010) 3924–3929.
[80] A.W. Rutherford, J.E. Mullet, A.R. Crofts, Measurement of the midpoint potential of the pheophytin acceptor of photosystem II, FEBS Lett. 123 (1981) 235–237.
[81] A. Tanaka, Y. Fukushima, N. Kamiya, Two different structures of the oxygen-evolving complex in the same polypeptide frameworks of photosystem II, J. Am. Chem. Soc. 139 (2017) 1718–1721.
[82] A. Ben Fredj, Z. Ben Lakhdar, M.F. Ruiz-López, Six-coordination in chlorophylls: the fundamental role of dispersion energy, Chem. Phys. Lett. 472 (2009) 243–247.
[83] W.D. Swingley, M. Chen, P.C. Cheung, A.L. Conrad, L.C. Dejesa, J. Hao, B. M. Honchak, L.E. Karbach, A. Kurdoglu, S. Lahiri, S.D. Mastrian, H. Miyashita, L. Page, P. Ramakrishna, S. Satoh, W.M. Sattley, Y. Shimada, H.L. Taylor, T. Tomo, T. Tsuchiya, et al., Niche adaptation and genome expansion in the chlorophyll d-producing cyanobacterium Acaryochloris marina, Proc. Natl. Acad. Sci. U. S. A. 105 (2008) 2005–2010.
[84] V.M. Ramesh, K. Gibasiewicz, S. Lin, S.E. Bingham, A.N. Webber, Bidirectional electron transfer in photosystem I: accumulation of A0- in a-side or B-side mutants of the axial ligand to chlorophyll A0, Biochemistry 43 (2004) 1369–1375.
[85] V.M. Ramesh, K. Gibasiewicz, S. Lin, S.E. Bingham, A.N. Webber, Replacement of the methionine axial ligand to the primary electron acceptor A0 slows the A0-reoxidation dynamics in photosystem I, Biochim. Biophys. Acta Bioenerg. 1767 (2007) 151–160.
[86] N. Dashdorj, W. Xu, R.O. Cohen, J.H. Golbeck, S. Savikhin, Asymmetric electron transfer in cyanobacterial photosystem I: charge separation and secondary electron transfer dynamics of mutations near the primary electron acceptor A0, Biophys. J. 88 (2005) 1238–1249.

[87] W. Giera, K. Gibasiewicz, V.M. Ramesh, S. Lin, A. Webber, Electron transfer from $A0^{-}$ to A1 in photosystem I from Chlamydomonas reinhardtii occurs in both the a and B branch with 25-30-ps lifetime, Phys. Chem. Chem. Phys. 11 (2009) 5186–5191.
[88] G.E. Milanovsky, V.V. Ptushenko, J.H. Golbeck, A.Y. Semenov, D.A. Cherepanov, Molecular dynamics study of the primary charge separation reactions in photosystem I: effect of the replacement of the axial ligands to the electron acceptor A0, Biochim. Biophys. Acta Bioenerg. 2014 (1837) 1472–1483.
[89] J. Sun, S. Hao, M. Radle, W. Xu, I. Shelaev, V. Nadtochenko, V. Shuvalov, A. Semenov, H. Gordon, A. van der Est, J.H. Golbeck, Evidence that histidine forms a coordination bond to the A0A and A0B chlorophylls and a second H-bond to the A1A and A1B phylloquinones in M688HPsaA and M668HPsaB variants of Synechocystis sp PCC 6803, Biochim. Biophys. Acta Bioenerg. 2014 (1837) 1362–1375.
[90] S. Santabarbara, I. Kuprov, O. Poluektov, A. Casal, C.A. Russell, S. Purton, M.C. W. Evans, Directionality of electron-transfer reactions in photosystem i of prokaryotes: universality of the bidirectional electron-transfer model, J. Phys. Chem. B 114 (2010) 15158–15171.
[91] T. Berthold, E. Donner Von Gromoff, S. Santabarbara, P. Stehle, G. Link, O. G. Poluektov, P. Heathcote, C.F. Beck, M.C. Thurnauer, G. Kothe, Exploring the electron transfer pathways in photosystem i by high-time-resolution electron paramagnetic resonance: observation of the B-side radical pair P 700+a 1B- in whole cells of the deuterated green alga Chlamydomonas reinhardtii at cryogenic temper, J. Am. Chem. Soc. 134 (2012) 5563–5576.
[92] S. Santabarbara, I. Kuprov, W.V. Fairclough, S. Purton, P.J. Hore, P. Heathcote, M.C.W. Evans, Bidirectional electron transfer in photosystem I: determination of two distances between P700+ and A1- in spin-correlated radical pairs, Biochemistry 44 (2005) 2119–2128.
[93] S. Santabarbara, I. Kuprov, P.J. Hore, A. Casal, P. Heathcote, M.C.W. Evans, Analysis of the spin-polarized electron spin echo of the [P 700+A1-] radical pair of photosystem I indicates that both reaction center subunits are competent in electron transfer in cyanobacteria, green algae, and higher plants, Biochemistry 45 (2006) 7389–7403.
[94] M. Byrdin, S. Santabarbara, F. Gu, W.V. Fairclough, P. Heathcote, K. Redding, F. Rappaport, Assignment of a kinetic component to electron transfer between iron-sulfur clusters FX and FA/B of photosystem I, Biochim. Biophys. Acta Bioenerg. 1757 (2006) 1529–1538.
[95] T. Förster, Zwischenmolekulare Energiewanderung und Fluoreszenz, Ann. Phys. 437 (1948) 55–75.
[96] M. Byrdin, P. Jordan, N. Krauss, P. Fromme, D. Stehlik, E. Schlodder, Light harvesting in photosystem I: modeling based on the 25-Å structure of photosystem I from Synechococcus elongatus, Biophys. J. 83 (2002) 433–457.
[97] M. Yang, A. Damjanović, H.M. Vaswani, G.R. Fleming, Energy transfer in photosystem I of cyanobacteria Synechococcus elongatus: model study with structure-based semi-empirical Hamiltonian and experimental spectral density, Biophys. J. 85 (2003) 140–158.
[98] T. Kramer, M. Noack, J.R. Reimers, A. Reinefeld, M. Rodríguez, S. Yin, Energy flow in the photosystem I supercomplex: comparison of approximative theories with DM-HEOM, Chem. Phys. 515 (2018) 262–271.
[99] P. Akhtar, I. Caspy, P.J. Nowakowski, T. Malavath, N. Nelson, H.S. Tan, P. H. Lambrev, Two-dimensional electronic spectroscopy of a minimal photosystem I complex reveals the rate of primary charge separation, J. Am. Chem. Soc. 143 (2021) 14601–14612.
[100] R.C. Jennings, G. Zucchelli, R. Croce, F.M. Garlaschi, The photochemical trapping rate from red spectral states in PSI-LHCI is determined by thermal activation of energy transfer to bulk chlorophylls, Biochim. Biophys. Acta Bioenerg. 1557 (2003) 91–98.
[101] B. Gobets, I.H.M. Van Stokkum, F. Van Mourik, J.P. Dekker, R. Van Grondelle, Excitation wavelength dependence of the fluorescence kinetics in photosystem I particles from Synechocystis PCC 6803 and Synechococcus elongatus, Biophys. J. 85 (2003) 3883–3898.
[102] M. Russo, A.P. Casazza, G. Cerullo, S. Santabarbara, M. Maiuri, Direct evidence for excitation energy transfer limitations imposed by low-energy chlorophylls in photosystem I-light harvesting complex i of land plants, J. Phys. Chem. B 125 (2021) 3566–3573.
[103] K.J. Riley, T. Reinot, R. Jankowiak, P. Fromme, V. Zazubovich, Red antenna states of photosystem I from cyanobacteria Synechocystis PCC 6803 and Thermosynechococcus elongatus: single-complex spectroscopy and spectral hole-burning study, J. Phys. Chem. B 111 (2007) 286–292.
[104] V. Zazubovich, S. Matsuzaki, T.W. Johnson, J.M. Hayes, P.R. Chitnis, G.J. Small, Red antenna states of photosystem I from cyanobacterium Synechococcus elongatus: a spectral hole burning study, Chem. Phys. 275 (2002) 47–59.
[105] A. Kimura, H. Kitoh-Nishioka, T. Aota, T. Hamaguchi, K. Yonekura, K. Kawakami, K. Shinzawa-Itoh, N. Inoue-Kashino, K. Ifuku, E. Yamashita, Y. Kashino, S. Itoh, Theoretical model of the far-red-light-adapted photosystem I reaction Center of Cyanobacterium Acaryochloris marina using chlorophyll d and the effect of chlorophyll exchange, J. Phys. Chem. B 126 (2022) 4009–4021.